

One dimensional hopping model - interplay of resistor-network and Sinai spreading

Notes by Daniel Hurowitz

Department of Physics, Ben-Gurion University of the Negev, P.O.B. 653, Beer-Sheva 84105, Israel

===== [1] Background

Theoretical framework

There is a recent interest in “glassy” systems that have log-wide distribution of relaxation rates [1]. For example we note recent works regarding electron dynamics where the effective model is essentially the same as a *random walk on a disordered lattice* [2, 3]. In such type of model there is a percolation-related crossover to sub-diffusion (in one dimension), or to variable-range-hopping type diffusion (in general) [4]. This crossover is reflected in the spectral properties of the system. An equivalent point of view regarding percolation is the continuous time random walk (CTRW) with a broad distribution of waiting times [5]. The more general problem of *random walk in random environment*, where transitions between sites are allowed to be asymmetric, has been explored by Sinai [6], Derrida [7], and followers [5, 8]. Focusing on one-dimensional systems, it turns out that for any small amount of disorder an unbiased spreading becomes sub-diffusive. For bias that exceeds a non-zero threshold there is a *sliding transition*, and the drift velocity becomes non-zero. Considering an N -site ring geometry, we ask what are the implications of the percolation and of the sliding transitions on the relaxation modes of such topologically closed system. A complementary question regarding the “delocalization” of eigenstates of non-Hermitian quantum Hamiltonians has been addressed by Hatano, Nelson, and followers [9–11]. Their main achievement is the realization that the complex spectrum of the non-Hermitian hamiltonian can be deduced from the real spectrum of an associated Hermitian hamiltonian. Various improvements on the method and ensuing analytical results were obtained. For example, the spectrum in the thermodynamic limit was found in [12]. An equation for the position of the eigenvalues in the complex plane and the density of states was found in [13]. Results for special models of one impurity and one way dynamics (maximally asymmetric transition rates) were obtained in [14].

The “Hatano-Nelson” model describes vortex depinning in superconductors [9, 10], certain types of DNA denaturation [15, 16] and non conservative population biology [17].

We show below that for a conservative “random walk” dynamics the implied spectral properties are dramatically different.

Applications

Conservative processes: Molecular motors [18, 19], fluid dynamics [20].

===== [2] Introduction

The conventional view of variable-range-hopping is based on the assumption that the rates of transitions are *symmetric* but have log-wide distribution as in glassy systems. Namely, the rate at the n th bond is written as

$$g_n = \text{rate of transition} = \exp(-\mathcal{B}_n) \quad (1)$$

where the barriers \mathcal{B}_n have (say) a box distribution. Consequently a resistor-network analysis is most appropriate for the analysis, leading to an Ohmic result for the current, namely $I \propto 1/L$, where L is the length of the sample, but the prefactor is exponentially small.

Contrary to that Sinai has considered a model where the rates are *asymmetric*. The asymmetry of transitions in the n th bond is characterized by

$$\mathcal{E}_n = \ln \left(\frac{\overrightarrow{w}_n}{\overleftarrow{w}_n} \right) \quad (2)$$

which we call “stochastic field”. At equilibrium $\mathcal{E}_n = (E_n - E_{n+1})/T$, where T is the temperature. More generally

we can define a stochastic potential

$$V_n = \sum_{n'=0}^n \mathcal{E}_{n'} \quad (3)$$

In non-equilibrium circumstances the telescopic correlations are likely to be broken, the sum becomes of order \sqrt{L} , and therefore $I \propto \exp(-\sqrt{L})$ due to this buildup of an activation barrier.

===== [3] The model, and main observations

Below we consider a 1D model where we have an interplay of resistor-network physics (due to random couplings) and Sinai physics (due to random stochastic field). Specifically we consider an N site ring with near-neighbor transitions. Each bond is characterized by two numbers:

$$[\text{e1}] \mathcal{B}_n = \text{barriers} = \text{random} \in [-\Delta, \Delta] \quad (4)$$

$$\mathcal{E}_n = \text{stochastic field} = \text{random} \in [s - \sigma, s + \sigma] \quad (5)$$

Accordingly the transition rates across the n^{th} bond are

$$[\text{e1}] \vec{w}_n = w_{n+1,n} = g_n e^{\mathcal{E}_n/2} = e^{-\mathcal{B}_n + \mathcal{E}_n/2} \quad (6)$$

$$\overleftarrow{w}_n = w_{n,n+1} = g_n e^{-\mathcal{E}_n/2} = e^{-\mathcal{B}_n - \mathcal{E}_n/2} \quad (7)$$

The average stochastic field s is called in the literature “affinity”. It can be written as $s = \text{Force}/T$, where the force is defined as the slope of the potential, and T is the temperature. The term “slope” is appropriate if we view our model as describing a periodic lattice with N -site unit cell. But we prefer to have in mind a ring geometry so the more appropriate notion is “stochastic motive force”:

$$S_{\circlearrowright} = \sum_{n \in \text{ring}}^N \mathcal{E}_n = Ns \quad (8)$$

What is the significance of a finite gap? The meaning of having a "gap" is that the relaxation is towards a localized NESS whose extension is L independent. The simplest example is $g = \infty$, for which the NESS is concentrated in a small triangular well. More generally if the NESS is localized we should expect a gap. In other words, if the gap vanishes then the decay times of the "non" NESS modes diverge, leading to a spatially extended NESS.

===== [4] Continuous models - general

To explain the observations we first consider three simpler continuous models of a ring of circumference L . In the continuous version, the dynamics is described by a diffusion equation with a drift term.

$$[e11] \frac{\partial \psi}{\partial t} = \frac{\partial}{\partial x} \left[D(x) \frac{\partial \psi}{\partial x} - v(x) \psi \right] \quad (9)$$

$$= \frac{\partial}{\partial x} \left[D(x) \frac{\partial \psi}{\partial x} \right] - \frac{\partial}{\partial x} [v(x) \psi] \quad (10)$$

Assuming that $D(x)$ and $v(x)$ are piecewise, the solution to the diffusion equation in each region is simply $\psi \sim e^{-\lambda t + ikx}$, inserting this in [equation \(9\)](#), we obtain the dispersion relation

$$\lambda = Dk^2 + ivk = D \left(k + \frac{iv}{2D} \right)^2 + \frac{v^2}{4D} \quad (11)$$

$$k_{\pm} = \frac{-iv \pm \sqrt{4\lambda D - v^2}}{2D} = \frac{-is}{2} \pm \sqrt{\frac{\lambda}{D} - \frac{s^2}{4}} \equiv \frac{-is}{2} \pm \tilde{k} \quad (12)$$

So, in each region the solution to [equation \(9\)](#) has the form

$$[e12] \psi(x) = A e^{ik_+ x} + B e^{ik_- x} = e^{\frac{v}{2D} x} \left(A e^{i \frac{\sqrt{4\lambda D - v^2}}{2D} x} + B e^{-i \frac{\sqrt{4\lambda D - v^2}}{2D} x} \right) \quad (13)$$

Details regarding matching the wave functions across interfaces where there is a jump in the values of v and D are given in the appendix. In the next three sections we consider several cases that are of special interest.

===== [5] Clean ring

The diffusion constant is constant, $D(x) = D$ and the drift velocity is $v = Ds$. By imposing periodic boundary conditions $\psi(0) = \psi(L)$, $\psi'(0) = \psi'(L)$, we have the secular equation

$$\cos \left(L \sqrt{\frac{\lambda}{D} - \frac{v^2}{4D}} \right) = \cosh \left(\frac{v}{2D} L \right) \quad (14)$$

we obtain the spectrum

$$[e14] \lambda = D \frac{4\pi^2 n^2}{L^2} + i \frac{2\pi v}{L} n, \quad n = 0, \pm 1, \pm 2, \dots \quad (15)$$

$$\lambda = \frac{v^2}{4D} \quad (16)$$

We see that there is a gap $\Delta = 4\pi^2/L^2$, which vanishes in the limit $L \rightarrow \infty$. The eigenvalue $\lambda = v^2/4D$ corresponds to an evanescent mode inside the gap.

If the ring is disconnected at a point, then we have a chain and Neumann boundary conditions apply, leading to the

eigenvalues

$$[e15] \lambda = D \frac{\pi^2 n^2}{L^2} + \frac{v^2}{4D}, \quad n = 0, 1, 2, \dots \quad (17)$$

$$\lambda = 0 \quad (18)$$

===== [6] Ring and scatterer

===== [6.1] The model

We have a ring with uniform drift velocity u and a diffusive scatterer, defined as

$$D(x) = \begin{cases} D_0, & |x| < a/2 \\ D, & |x| > a/2 \end{cases} \quad (19)$$

The strength of the scatterer can be written in dimensionless units

$$g \equiv \frac{a}{L} \cdot \frac{D}{D_0} \quad (20)$$

===== [6.2] The secular equation

The secular equation for the eigenvalues can be shown to be (see appendix)

$$[e18] \cos\left(L\sqrt{\frac{\lambda}{D} - s^2/4}\right) + \frac{1}{2} \frac{aD}{D_0} \frac{\lambda}{\sqrt{\frac{\lambda}{D} - s^2/4}} \sin\left(L\sqrt{\frac{\lambda}{D} - s^2/4}\right) = \cosh\left(\frac{sL}{2}\right) \quad (21)$$

and in terms of dimensionless variables

$$g \equiv \frac{a}{L} \cdot \frac{D}{D_0} \quad (22)$$

$$z \equiv \tilde{k}L, \quad \mathcal{S} \equiv sL \quad (23)$$

$$\lambda = D \left(\tilde{k}^2 + \frac{s^2}{4} \right) \quad (24)$$

the secular equation can be written as

$$[e19] \cos(z) + g \frac{z^2 + (\frac{\mathcal{S}}{2})^2}{2z} \sin(z) = \cosh\left(\frac{\mathcal{S}}{2}\right) \quad (25)$$

===== [6.3] The spectrum

To characterize the spectrum vs. s , it is good to keep in mind two limiting cases. When $g = 0$, we have a clean ring, and all eigenvalues are complex and they form a gapless continuum. When $g = \infty$, we have a chain, where all the eigenvalues are real. In this case there is a gapped continuum that begins at $\Delta = s^2/4$.

For finite g , the spectrum is gapped, however a "bubble" of complex eigenvalues can appear in the continuum. We obtain an analytical expression for the gap when the spectrum is real and prove that the gap is finite even when there are complex eigenvalues in the spectrum.

Let us assume that λ is real. For given \mathcal{S} , the left hand side of the secular equation [equation \(21\)](#) is oscillatory, provided $\lambda > \mathcal{S}^2/4$, otherwise, the trigonometric functions become hyperbolic. The oscillations are within an envelope function $\kappa(\lambda)$,

$$\kappa(\lambda) = \sqrt{1 + \frac{g^2 \lambda^2}{4\lambda - \mathcal{S}^2}} \quad (26)$$

There are real solutions to the secular equation as long as the envelope function satisfies

$$\kappa(\lambda) > \cosh\left(\frac{\mathcal{S}}{2}\right) \quad (27)$$

which leads to the expression for the gap, provided that the spectrum is entirely real ([Fig. 1](#)),

$$[\text{e17}] \operatorname{Re}[\lambda] \geq \frac{2 \sinh^2(\mathcal{S}/2)}{g^2} \left[1 + \sqrt{1 - \frac{g^2 \mathcal{S}^2}{4 \sinh^2(\mathcal{S}/2)}} \right] = \Delta(s) \quad (28)$$

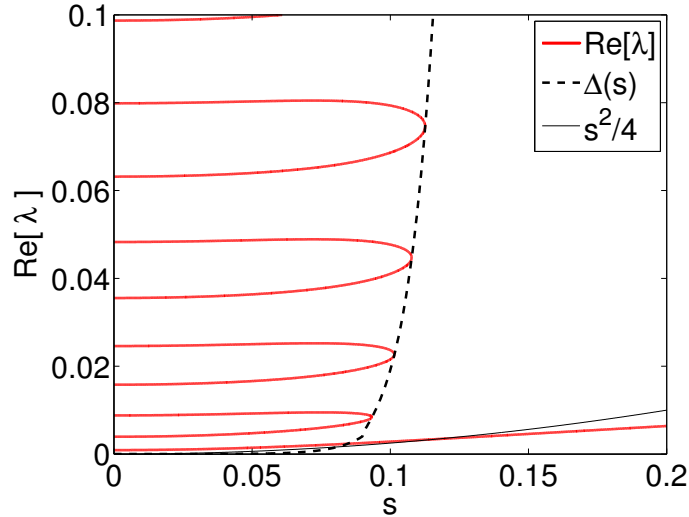


FIG. 1: The real part of the eigenvalues for an $L = 100$, $D = 1$ ring with a single diffusion barrier with $g = 10^3$ plotted vs. the affinity s . The dashed black line is [equation \(28\)](#), which is the value of the gap and also indicates where the eigenvalues become complex. Notice that at the bottom of the band there is an eigenvalue that is always real. This plot was generated by producing a contour plot of [equation \(21\)](#) for real λ 's, it shows only real eigenvalues.

When \mathcal{S} increases such that $\cosh(\mathcal{S}/2) > \kappa(\lambda)$, a complex "bubble" of eigenvalues appears. The bubble structure is due to the fact that the envelope function $\kappa(\lambda)$ has a global minimum at $\lambda_{\min} = \mathcal{S}^2/2$, so for $\lambda > \lambda_{\min}$ the envelope function grows monotonically and will eventually intersect with $\cosh(\mathcal{S}/2)$. This scenario is illustrated in [Fig. 2](#). The minimum value of the envelope function is

$$\kappa_{\min} = \sqrt{1 + \left(\frac{g\mathcal{S}}{2}\right)^2} \quad (29)$$

The critical value \mathcal{S}_g such that for $\mathcal{S} > \mathcal{S}_g$ there are complex eigenvalues in the spectrum is determined by the transcendental equation

$$1 + \left(\frac{g\mathcal{S}}{2}\right)^2 = \cosh^2\left(\frac{\mathcal{S}}{2}\right) \quad (30)$$

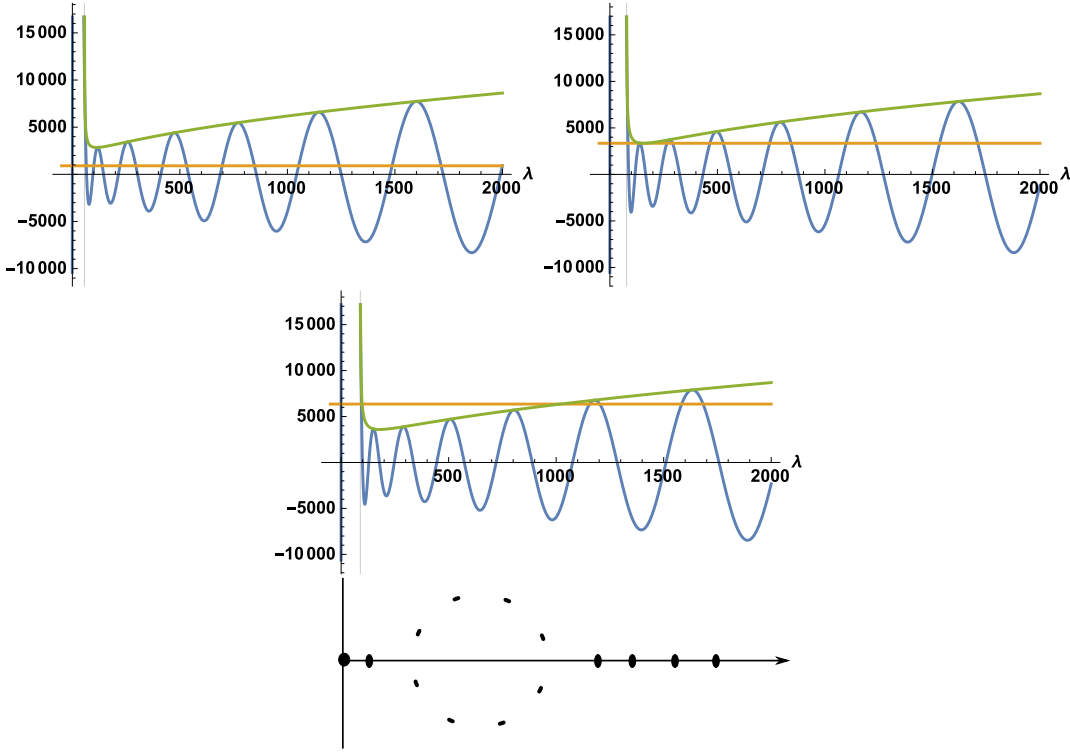


FIG. 2: The secular equation $f(\lambda) = \cosh(S/2)$ for $g = 380$, so $S_g = 17.6$. Top row: (left) $S = 15$, all eigenvalues are real. (right) $S = S_g$, marginal case. Middle row: (left) $S = 19$, the fully developed scenario, where the spectrum is initially real, then there is a "bubble" of complex eigenvalues and then the spectrum becomes real again. The high eigenvalues correspond to modes that decay very fast. Intuitively, since the high eigenvalues decay quickly, they cannot complete a trip around the ring before they decay, so they must be real. The blue line is the oscillating part of the secular equation. The green line is the envelop function and the horizontal orange line is $\cosh(S/2)$. In the bottom row we draw a schematic diagram of the spectrum in the complex plane of λ , corresponding to the fully developed scenario.

===== [6.4] Proof the gap is finite

To show that the gap remains finite even when there are complex eigenvalues, it is more convenient to use the second form of the secular equation where the wave vector is $z = x + iy$. The eigenvalues can be expressed in the following form

$$\lambda = (x + iy)^2 + \left(\frac{S}{2}\right)^2 = x^2 - y^2 + \left(\frac{S}{2}\right)^2 + 2ixy \quad (31)$$

There is a trivial eigenvalue at $x = 0$, $y = S/2$. To show that the gap is finite, it is sufficient to show that for $x \neq 0$, $y < S/2$. Inserting $z = x + iy$, the secular equation splits into two equations (for real and imaginary parts). The real part of equation (25) is

$$[e20] \cos(x) \left[\cosh(y) - gy \sinh(y) \frac{x^2 + y^2 - S^2/4}{2(x^2 + y^2)} \right] + \sin(x) \left[gx \cosh(y) \frac{x^2 + y^2 + S^2/4}{2(x^2 + y^2)} \right] = \cosh\left(\frac{S}{2}\right) \quad (32)$$

This equation has the form $A(x, y) \sin(x) + B(x, y) \cos(x) = \cosh(S/2)$. For finite $x = x_1$, y_1 is determined by the condition that the envelope of the function intersects with $\cosh(S/2)$

$$\sqrt{A^2 + B^2} = \cosh(S/2) \quad (33)$$

To prove that $y_1 < \mathcal{S}/2$ it is enough to show that for $y = \mathcal{S}/2$ the envelope satisfies $\sqrt{A^2 + B^2} > \cosh(\mathcal{S}/2)$. Assume that $g \gg 1$ and $\mathcal{S} \gg \mathcal{S}_g$, in this case there is a large bubble of complex eigenvalues so the gap is complex. Also, we can approximate $\cosh y \approx \sinh y \approx e^y$ and $\cosh(\mathcal{S}/2) \approx e^{\mathcal{S}/2}$. In this limit the envelope is

$$\frac{g}{2} e^y \sqrt{x^2 + y^2} \sqrt{1 + \frac{\mathcal{S}^2(x^2 - y^2 + \mathcal{S}^2)}{2(x^2 + y^2)}} \Big|_{y=\mathcal{S}/2} = \frac{ge^{\mathcal{S}/2}}{2} \sqrt{x^2 + (\mathcal{S}/2)^2} \sqrt{1 + \frac{\mathcal{S}^2(x^2 + 3(\mathcal{S}/2)^2)}{2(x^2 + (\mathcal{S}/2)^2)}} > e^{\mathcal{S}/2} \quad (34)$$

so the solution must be $y < \mathcal{S}/2$.

===== [7] Ring and σ

===== [7.1] The model

The ring is divided in to two segments with drift velocities defined

$$v(x) = \begin{cases} v_1 = D(s + \sigma), & 0 < x < L/2 \\ v_2 = D(s - \sigma), & L/2 < x < L \end{cases} \quad (35)$$

===== [7.2] The secular equation

The secular equation for the eigenvalues can be shown to be (see appendix)

$$[e20] \cosh\left(\frac{\mathcal{S}}{2}\right) = \cos\left(\frac{L}{4}\sqrt{4\lambda - (s - \sigma)^2}\right) \cos\left(\frac{L}{4}\sqrt{4\lambda - (s + \sigma)^2}\right) - \quad (36)$$

$$- \frac{(4\lambda - s^2 + \sigma^2)}{\sqrt{4\lambda - (s - \sigma)^2}\sqrt{4\lambda - (s + \sigma)^2}} \sin\left(\frac{L}{4}\sqrt{4\lambda - (s - \sigma)^2}\right) \sin\left(\frac{L}{4}\sqrt{4\lambda - (s + \sigma)^2}\right) \quad (37)$$

or, in terms of dimensionless variables, $\mathcal{S} = sL$, $\sigma := \sigma L$

$$[e21] \cosh\left(\frac{\mathcal{S}}{2}\right) = \cos\left[\frac{1}{2}\sqrt{z^2 - \left(\frac{\sigma}{2}\right)^2 - \frac{\sigma\mathcal{S}}{2}}\right] \cos\left[\frac{1}{2}\sqrt{z^2 - \left(\frac{\sigma}{2}\right)^2 + \frac{\sigma\mathcal{S}}{2}}\right] - \quad (38)$$

$$- \left(z^2 + \left(\frac{\sigma}{2}\right)^2\right) \frac{\sin\left[\frac{1}{2}\sqrt{z^2 - \left(\frac{\sigma}{2}\right)^2 - \frac{\sigma\mathcal{S}}{2}}\right]}{\sqrt{z^2 - \left(\frac{\sigma}{2}\right)^2 - \frac{\sigma\mathcal{S}}{2}}} \frac{\sin\left[\frac{1}{2}\sqrt{z^2 - \left(\frac{\sigma}{2}\right)^2 + \frac{\sigma\mathcal{S}}{2}}\right]}{\sqrt{z^2 - \left(\frac{\sigma}{2}\right)^2 + \frac{\sigma\mathcal{S}}{2}}}$$

===== [7.3] The spectrum

We first consider two limiting cases, $\mathcal{S} = 0$ and $\mathcal{S} \gg \sigma$ and then the general case. For $\mathcal{S} = 0$, the secular equation can be written as

$$[e22] \tan^2\left(\frac{1}{4}\sqrt{4\lambda - \sigma^2}\right) = \frac{4\lambda - \sigma^2}{4\lambda + \sigma^2} \quad (39)$$

There is the trivial solution at $\lambda = 0$, the next solution is at $\lambda = \sigma^2/4$ so there is a finite gap independent of L , followed by a "continuum", see Fig. 3.

For $\mathcal{S} \gg \sigma$, we neglect σ in the secular equation and obtain the secular equation for a clean ring,

$$\cos\left(\frac{1}{2}\sqrt{4\lambda - \mathcal{S}^2}\right) = \cosh\left(\frac{\mathcal{S}}{2}\right) \quad (40)$$

That is, the spectrum is gapless ($\Delta \sim 1/L^2$) and complex.

For intermediate values of \mathcal{S} , the spectrum can be divided into three regions. For $\lambda > (\mathcal{S} + \sigma)^2/4$, all the trigonometric functions are oscillatory, resulting in a continuum. Since the envelope function is bounded in this region, the eigenvalues are complex.

For $(\mathcal{S} - \sigma)^2/4 < \lambda < (\mathcal{S} + \sigma)^2/4$ the trigonometric functions whose argument is $\sqrt{\lambda - (\mathcal{S} + \sigma)^2/4}$ become hyperbolic. The oscillations ensure that the eigenvalues form a continuum, and the hyperbolic functions form an envelope that is unbounded, so the eigenvalues may be real, depending on \mathcal{S} . In order for there to be real eigenvalues, there must be oscillations, this happens only if $\sigma > 4\pi$. The envelope function is

$$\kappa(\lambda) = \left(\left[\cosh \left(\frac{1}{4} \sqrt{|4\lambda - (s + \sigma)^2|} \right) \right]^2 + \left[\sinh \left(\frac{1}{4} \sqrt{|4\lambda - (s + \sigma)^2|} \right) \frac{(4\lambda - s^2 + \sigma^2)}{\sqrt{4\lambda - (s - \sigma)^2} \sqrt{|4\lambda - (s + \sigma)^2|}} \right]^2 \right)^{1/2} \quad (41)$$

For $\lambda < (\mathcal{S} - \sigma)^2/4$ all the terms are hyperbolic, so there is at most one solution in this region.

The gap decreases from $\sigma^2/4$ to $(\mathcal{S} - \sigma)^2/4$ until some point $\mathcal{S} = \sigma - \epsilon$, then the gap becomes complex and increases until $\mathcal{S} = \sigma$ from which point the gap closes. I don't know how to determine ϵ , however it arises because at $\mathcal{S} = \sigma$, the envelope is equal to $\cosh(\mathcal{S}/2)$ at $\lambda = 0$ and is a monotonically decreasing function of λ . Thus the first non trivial solution is for $\mathcal{S} < \sigma$. In any case, this solution is part of the continuum so we can deduce that $\epsilon \sim 1/L^2$.

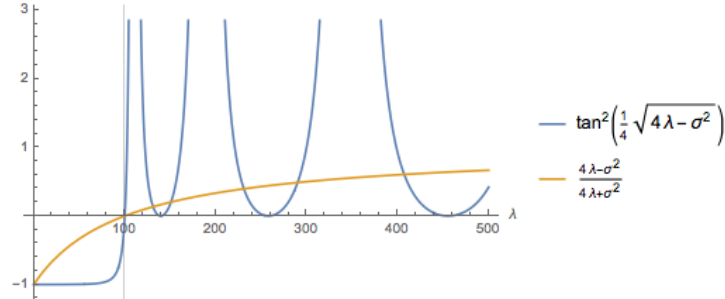


FIG. 3: Graphical solution of the secular equation [equation \(39\)](#) for $\mathcal{S} = 0$ and $\sigma = 20$, depicting the finite gap at $\lambda = 100$

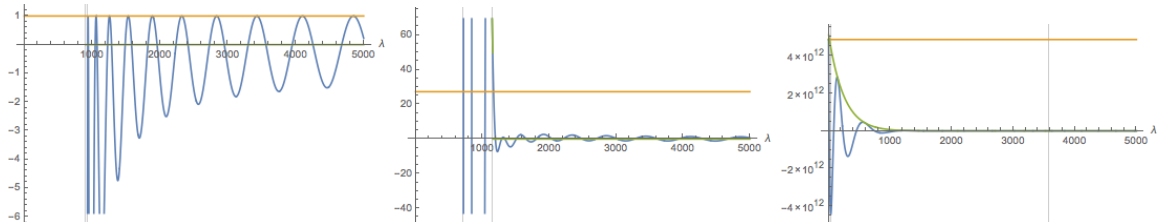


FIG. 4: Graphical representation of the secular equation. The horizontal orange line is $\cosh(\mathcal{S}/2)$. Top: $\mathcal{S} = 0$ (corresponds to [Fig. 3](#)), there is a gap $\Delta = \sigma^2/4$ between $\lambda = 0$ and a real continuum, Middle: $\mathcal{S} < \sigma$, there is a gap, followed by a real continuum, followed by a complex continuum. Bottom: $\mathcal{S} = \sigma$ the gap vanishes, followed by a complex continuum.

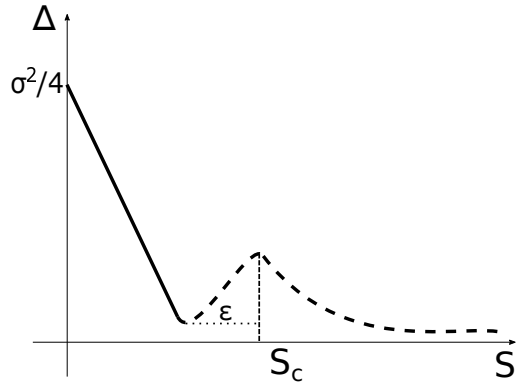


FIG. 5: Schematic drawing of the gap Δ vs. S . Solid line indicates a real gap, dashed line indicates a complex gap.

[8] Tight binding models

In this section we present the results for the corresponding tightbinding models.

[8.1] Tight binding clean ring

Consider a discrete lattice of length L with lattice constant a , such that $L = Na$. Periodic boundary conditions are imposed. The rate equation is diagonal in the momentum basis, thus the dispersion relation for a clean ring is given by

$$\lambda(k) = 2 \cos\left(ika + \frac{sa}{2}\right) - 2 \cosh\left(\frac{sa}{2}\right) \quad (42)$$

The dispersion relation can be inverted to obtain k_{\pm} (we take the first branch)

$$k_{\pm} = \frac{is}{2} \pm \frac{1}{a} \arccos\left[\frac{\lambda}{2} + \cosh\left(\frac{sa}{2}\right)\right] \quad (43)$$

The secular equation for periodic boundary conditions is just as in the continuous model,

$$(k_- - k_+) \left(1 - e^{ik_- L} - e^{ik_+ L} + e^{i(k_- + k_+)L}\right) = 0 \quad (44)$$

Which yields the equation,

$$\cos\left[\frac{L}{a} \arccos\left(\frac{\lambda}{2} + \cosh\frac{sa}{2}\right)\right] = \cosh\left(\frac{sL}{2}\right) \quad (45)$$

The solutions are

$$[e23] \lambda_n = 2 \cosh\left(\frac{\mathcal{S}}{2N}\right) \left[\cos\left(\frac{2\pi n}{N}\right) - 1 \right] + 2i \sinh\left(\frac{\mathcal{S}}{2N}\right) \sin\left(\frac{2\pi n}{N}\right) \quad (46)$$

where $s = \mathcal{S}/Na$. The gap is give by the first non zero eigenvalue

$$[e24] \Delta = \lambda_1 \approx \frac{4\pi^2}{N^2} \cosh\left(\frac{as}{2}\right) + i \frac{4\pi}{N} \sinh\left(\frac{as}{2}\right) \quad (47)$$

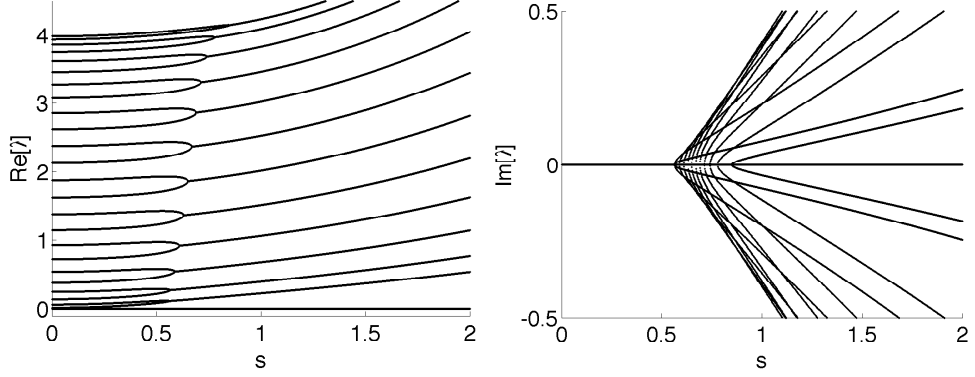
[8.2] Tight binding ring+ g


FIG. 6: The eigenvalues for an $N = 25$ ring with a single diffusion barrier with $g = \exp(-7.5)$ plotted vs. the affinity s .

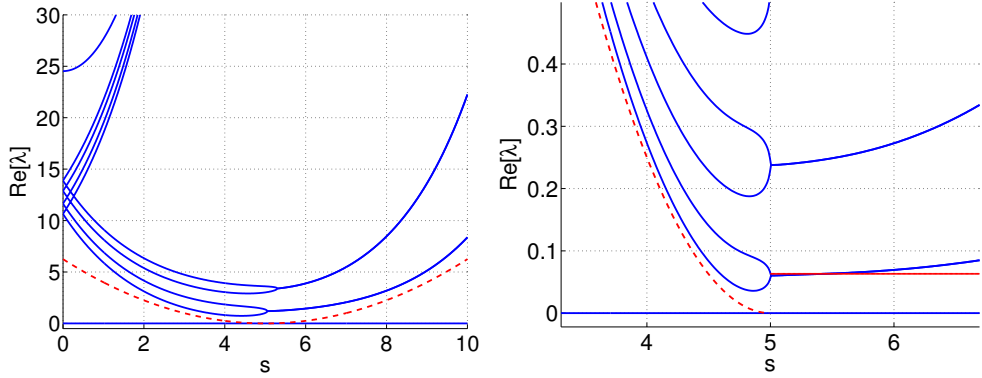
[8.3] Tight binding ring + σ


FIG. 7: Left panel: The eigenvalues for an $N = 10$ ring with two drift regions $\sigma = 5$ plotted vs. the affinity s . Right panel: The same, but for $N = 100$, focusing on the lower bands. The horizontal red line is $\text{Re}[\lambda] = 16\pi^2 D/N^2$.

[8.4] Tight binding ring + well

We consider a ring that has a triangular well with slope σ .

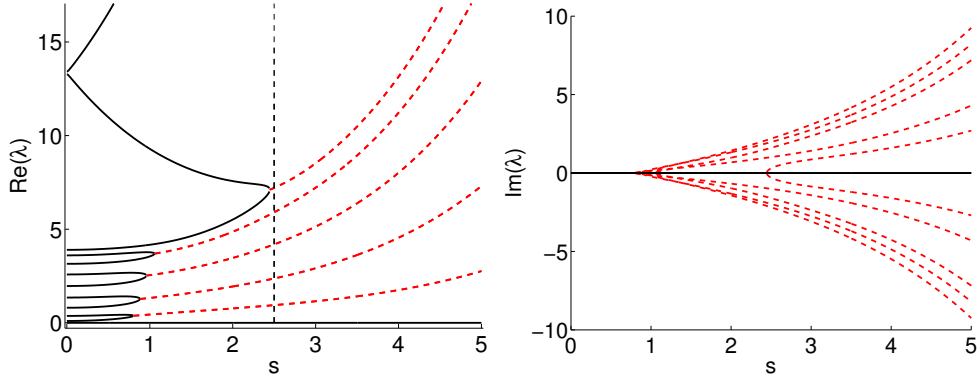


FIG. 8: Left panel: The eigenvalues for an $N = 12$ ring with a well with slope $\sigma = 5$ plotted vs. the affinity s . Solid black lines indicate the eigenvalues are real. Dashed red indicate they are complex.

===== [9] Tight binding with disorder

===== [9.1] The model

Below we consider a 1D model where we have an interplay of resistor-network physics (due to random couplings) and Sinai physics (due to random stochastic field). Specifically we consider an N site ring with near-neighbor transitions. Each bond is characterized by two numbers:

$$[e1] \mathcal{B}_n = \text{barriers} = \text{random} \in [-\Delta, \Delta] \quad (48)$$

$$\mathcal{E}_n = \text{stochastic field} = \text{random} \in [s - \sigma, s + \sigma] \quad (49)$$

Accordingly the transition rates across the n^{th} bond are

$$[e1] \vec{w}_n = w_{n+1,n} = g_n e^{\mathcal{E}_n/2} = e^{-\mathcal{B}_n + \mathcal{E}_n/2} \quad (50)$$

$$\overleftarrow{w}_n = w_{n,n+1} = g_n e^{-\mathcal{E}_n/2} = e^{-\mathcal{B}_n - \mathcal{E}_n/2} \quad (51)$$

The average stochastic field s is called in the literature “affinity”. It can be written as $s = \text{Force}/T$, where the force is defined as the slope of the potential, and T is the temperature. The term “slope” is appropriate if we view our model as describing a periodic lattice with N -site unit cell. But we prefer to have in mind a ring geometry so the more appropriate notion is “stochastic motive force”:

$$\mathcal{S} = \sum_{n \in \text{ring}}^N \mathcal{E}_n = Ns \quad (52)$$

===== [9.2] Main observations

It is known from the work of Derrida [7] that there are ”phase transitions” when

$$[e2] \left\langle \left(\frac{\vec{w}}{\overleftarrow{w}} \right)^\mu \right\rangle = 1 \quad (53)$$

For our log-box model of disorder this equation becomes (see Fig. 11).

$$[e3] s_\mu = \frac{1}{\mu} \ln \left(\frac{\sinh(\mu\sigma)}{\mu\sigma} \right) \quad (54)$$

For example, for $\mu = 1/2$ the diffusion coefficient goes from sub ohmic to super ohmic, for $\mu = 1$ there is a transition from $v = 0$ to finite v and For $\mu = 2$ there is a transition from $D = \infty$ to finite D . These are properties of the steady state, yet remarkably they have fingerprints on the relaxation process as well. For example, if we count the number of complex eigenvalues vs. s we see that not all of the eigenvalues become complex. The spectrum begins to show complexity at $s_{1/2} =$ and the number of complex eigenvalues saturates at s_1 . We call this ”complexity saturation”.

If we look at the gap, then it becomes complex at $s_{1/2}$ and has a peak at s_1 . If there is off diagonal disorder, then the peak is diminished. We would like to establish whether there is a finite gap in the spectrum and how it scales with the system size N . The gap Δ in the spectrum is just the real part of the second largest eigenvalue. Our goal is to characterise the gap for the general disordered hopping model, see for example Fig. 10. At $s = s_{1/2}$ the gap becomes complex and at $s = s_1$ the gap reaches a peak value. It is easy to explain the large s behavior - which is just the clean ring limit. Recall (equation (46), equation (47)) that for a clean ring the eigenvalues are $\lambda_n \propto (n/N)^2$, hence $\Delta = \lambda_1 \sim 1/N^2$ and the integrated density of states $\mathcal{N}(\lambda) \propto N\lambda^{1/2}$. Near the peak it can be shown that $\mathcal{N}(\lambda) \propto N\lambda$, leading to $\Delta \sim 1/N$.

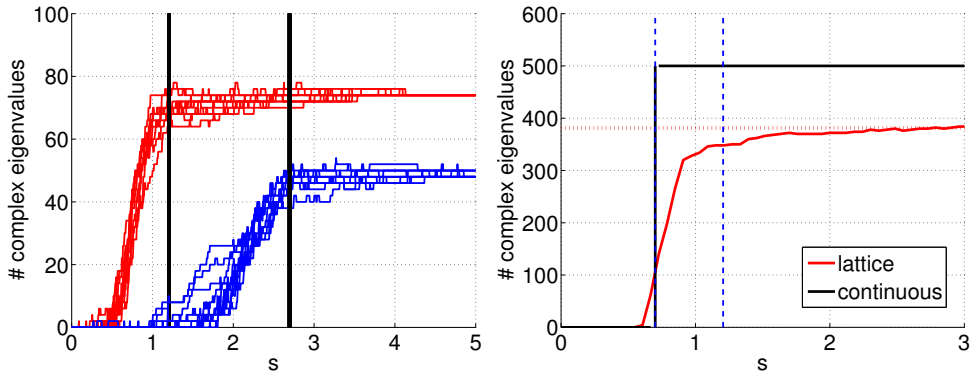


FIG. 9: Left: Number of complex eigenvalues vs. s for $N = 100$ sites. Each red line corresponds to a different realisation of field disorder with $\sigma = 3$ (red) and $\sigma = 5$ (blue), but $\Delta = 0$. The black vertical lines are at values of s at which the sliding transition occurs. Right: Number of complex eigenvalues vs. s for $N = 500$ sites and $\sigma = 5$ (red) vs. the result of the continuous problem(black step function) The vertical dashed lines are $s_{1/2}$ and s_1 . The dotted horizontal red line is the estimated saturation value, equation (115).

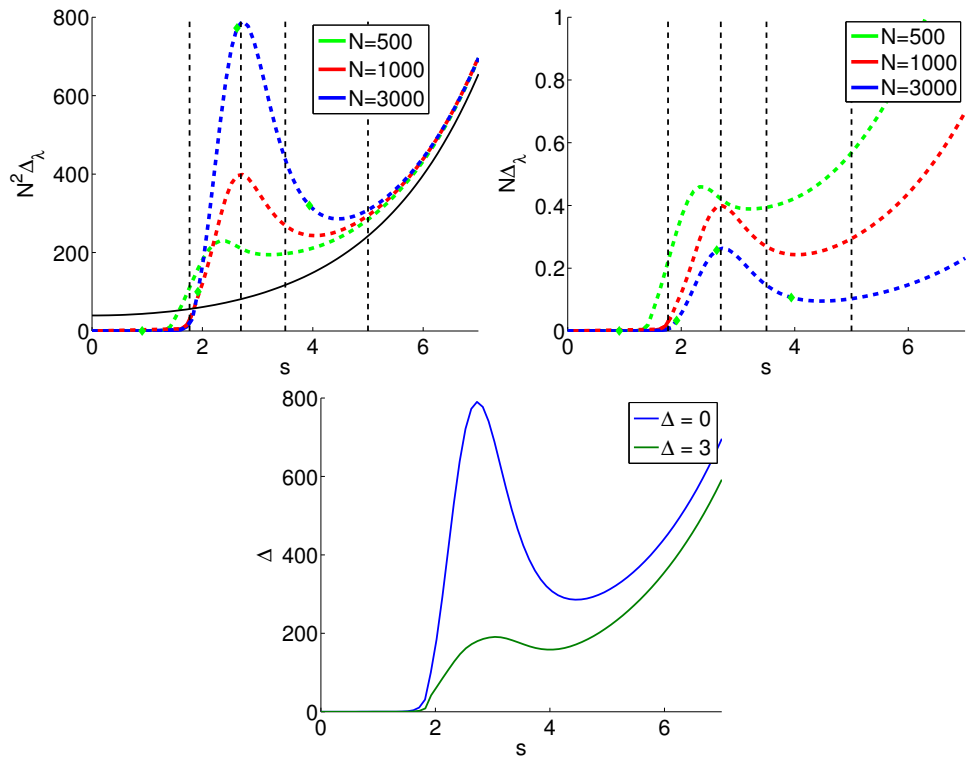


FIG. 10: Top row: Gap vs. s with disorder $\sigma = 5$. The dashed segment corresponds to a complex spectrum. The three lines corresponds to different values of N . The black line is $4\pi^2/N^2 \cosh(s/2)$, as in a clean ring. The vertical dashed lines are $s = s_{1/2}$, s_1 , s_2 and $s = s_\infty = \sigma$. On the left the gap is rescaled by N^2 , on the right by N , showing that near the peak $\Delta_\lambda \sim 1/N$ and for $s > s_\infty$, $\Delta_\lambda \sim 1/N^2$. Bottom panel: The gap vs. s for different values of off diagonal disorder, Δ , illustrating that the off diagonal disorder, or "glassiness" kills the gap.

===== [9.3] Scaled affinity, cumulants of the stochastic field

For stochastic fields that have a uniform distribution with width σ , equation (53) becomes

$$s_\mu = \frac{1}{\mu} \ln \left(\frac{\sinh(\mu\sigma)}{\mu\sigma} \right) \quad (55)$$

where s_μ is the scaled affinity. It is interesting that for large μ , it saturates and $s_\infty = \sigma$. In contrast, if the stochastic field has a normal distribution with standard deviation σ , then $s_\mu = (1/2)\sigma^2\mu$ and the scaled affinity is unbounded. The two models agree only for small μ (see Fig. 11). Note that $\text{var}[\text{box}] = \sigma^2/12$ and $\text{var}[\text{normal}] = \sigma^2$.

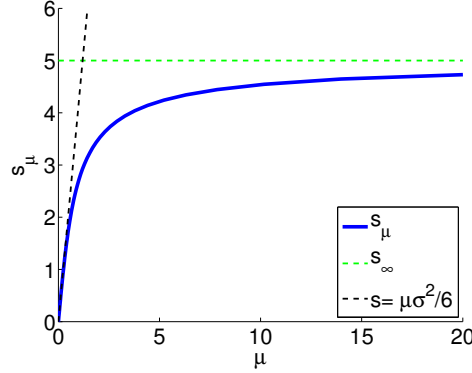


FIG. 11: The scaled affinity s_μ saturates at $s = s_\infty = \sigma$.

——— [9.4] Algorithm for analysis

Given an asymmetric and conservative matrix

$$W = -\text{diag}[\Gamma_{n-1}] + \text{offdiag}[g_n e^{\pm(s+\sigma_n)/2}] \quad (56)$$

The diagonal elements (decay rates) are determined by the conservativity requirement

$$\Gamma_n(s) = g_{n-1} e^{-(s+\sigma_{n-1})/2} + g_n e^{(s+\sigma_n)/2} \quad (57)$$

we take the following steps

1. Gauge away the field disorder, we are left with an asymmetric matrix of the form

$$e^{V/2} W e^{-V/2} = \tilde{W} = -\text{diag}[\Gamma_{n-1}(s)] + \text{offdiag}[g_n e^{\pm s/2}] \quad (58)$$

where the diagonal depends on s, σ and Δ . Note that the sum of each column of the gauged matrix is not zero.

2. Define the associated hermitian matrix by setting $s = 0$ on the off diagonal. Now we have the matrix

$$H = -\text{diag}[\Gamma_{n-1}(s)] + \text{offdiag}[g_n] \quad (59)$$

which is *symmetric and non conservative*. Note that the diagonal elements depend on s !

3. Calculate the eigenvalues of the associated Hermitian matrix, $\varepsilon_j(s)$.

4. The eigenvalues of the original, non hermitian problem are solutions to the secular equation

$$\prod_{j=1}^N (\lambda - \varepsilon_j(s)) = \left[\prod_{n=1}^N g_n \right] 2 \left(\cosh \left(\frac{sN}{2} \right) - 1 \right) \quad (60)$$

where λ is complex.

5. According to Thouless, the left hand side of the equation can be written as

$$e^{N/\xi} = \prod_{j=1}^N (\lambda - \varepsilon_j(s)) \quad (61)$$

where the inverse localization length

$$\kappa \equiv \xi^{-1} = \frac{1}{N} \sum_{j=1}^N \ln(|\lambda - \varepsilon_j(s)|) \quad (62)$$

is equivalent to a 2D electrostatic potential due to charges $q_j = \varepsilon_j(s)$ along the x axis. Once we determine the density of states, we can solve the electrostatic problem. This will allow us to determine when the eigenvalues are complex and whether there is a finite gap.

6. For weak disorder, the inverse localization length of the lower bands of the associated hermitian system can be calculated by FGR.

===== [9.5] Electrostatic analogy

According to Thouless, the inverse localization length κ is given by

$$\kappa(\lambda) = \frac{1}{N} \sum_{j=1}^N \ln(|\lambda - \varepsilon_j(s)|) \quad (63)$$

The inverse localization length is in fact the sum of point charges on a line in 2 dimensions. In the limit $N \rightarrow \infty$, the sum is replaced by an integral and κ can be expressed as an electrostatic potential. Using the notation $\lambda = z = x + iy$ and $\varepsilon_j = x'$,

$$\Phi = \varphi(x, y) + i\psi(x, y) = \int \ln(z - x') \rho(x') dx' \quad (64)$$

The real part is the electrostatic potential $\kappa = \varphi(x, y)$

$$[e65] \varphi(x, y) = \int \ln(|z - x'|) \rho(x') dx' = \frac{1}{2} \int \ln[(x - x')^2 + y^2] \rho(x') dx' \quad (65)$$

The imaginary part is the field lines

$$\psi(x, y) = \arg(z - x') \quad (66)$$

The non hermitian requirement that

$$\varphi(x) = \ln \left[2 \left(\cosh \left(\frac{sN}{2} \right) - 1 \right) \right] \quad (67)$$

defines an equipotential line.

The requirement

$$\psi(x, y) = 2\pi n, \quad n = 0, \pm 1, \pm 2, \dots \quad (68)$$

defines the field lines, that are perpendicular to the equipotential lines (this is a result of the Cauchy-Riemann equation). To determine the gap we need the intersection of the equipotential line with the field line that originates from the first point charge (lowest eigenvalue of the associated Hermitian problem).

[9.6] The Density of states of the associated Hermitian matrix

For weak disorder, $\mathcal{S} \gg \sigma$, the diagonal elements of the associated Hermitian matrix are large compared to the off-diagonal elements, $\gamma_n \gg 1$. Also, in this limit the diagonal elements are uncorrelated. As a result, their distribution is just a log-box distribution, i.e.

$$\rho(\varepsilon) = \frac{1}{\sigma\varepsilon}, \quad \sigma = \ln \frac{\varepsilon_{\max}}{\varepsilon_{\min}} \quad (69)$$

For strong disorder, $\mathcal{S} \ll \sigma$, the coupling terms cannot be neglected and also the decay rates are correlated. It has been shown [8] that for this kind of problem the density of states exhibits a "spectral condensate" at $\varepsilon = 0$ and not a "Lifshitz tail", See Fig. 12.

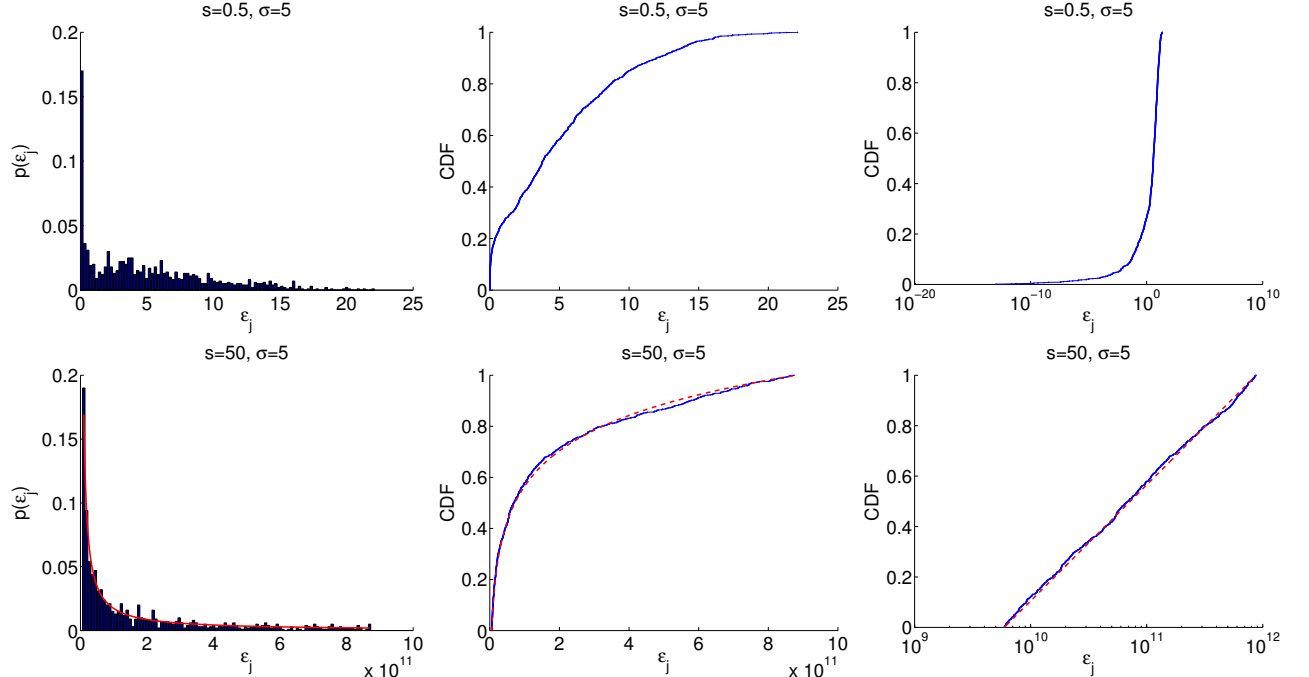


FIG. 12: Top row: Histogram and cumulative distribution function for strong disorder ($\mathcal{S} \ll \sigma$). Bottom row: Histogram and cumulative distribution function for weak disorder ($\mathcal{S} \gg \sigma$), the density of states is $\rho = (\sigma x)^{-1}$ (solid red line). The right hand column is the CDF of $\log(\varepsilon_j)$ to highlight the lower tail. The simulation is for $N = 1000$ sites, $\sigma = 5$ and $\mathcal{S} = 0.5, 50$.

[10] The spectrum of a disordered ring

We plot the equation

$$[e69] \sum_{j=1}^N \log(|\lambda - \varepsilon_j(s)|) = \log \left[2 \left(\cosh \left(\frac{sN}{2} \right) - 1 \right) \right] \quad (70)$$

The interesting behavior is at the bottom of the spectrum. Large values of λ simply correspond to a clean ring. The condition for complexity is that $\kappa < \log \left[2 \left(\cosh \left(\frac{sN}{2} \right) - 1 \right) \right]$. Focusing on the lower region of the spectrum we see that

1. For $s < s_{1/2}$, κ is convex with a minimum at the origin (the spectrum is real).
2. In the vicinity of the sliding transition $s \approx s_1$, κ is concave but very shallow (the spectrum is complex).
3. For large values of $s > s_1$, κ is concave with a minimum far from the origin (the spectrum is complex).

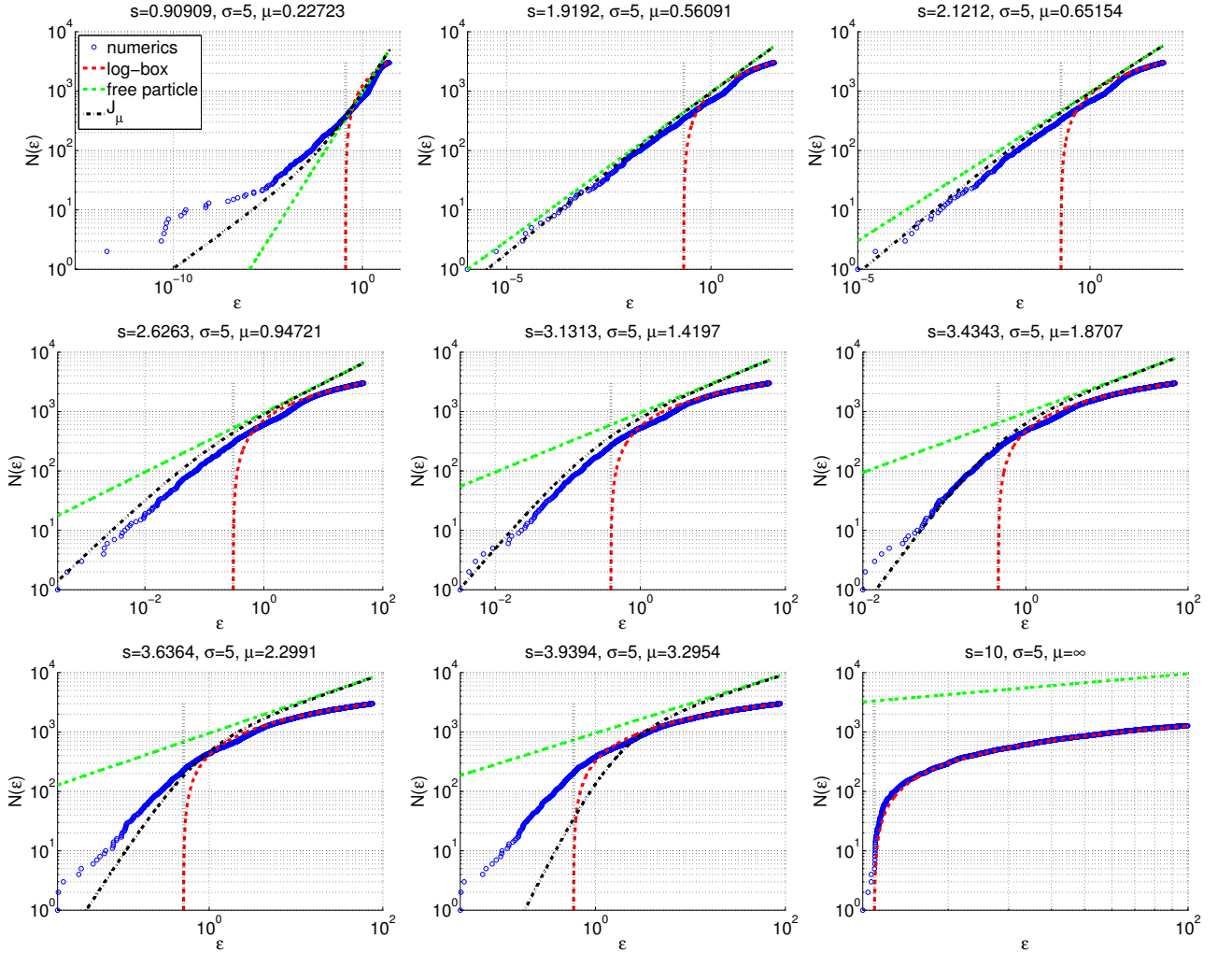


FIG. 13: Integrated density of states. The blue points are calculated from numerical diagonalization. The red line dashed curve corresponds to the log-box result (large s), equation (74). The black dashed-dot line is equation (102) and the green line is just a free particle equation (103). The vertical dotted line is $\epsilon = \exp[(s - \sigma)/2]$.

It is possible to obtain analytical expressions for the envelope function in the limits of weak and strong disorder, as will be shown in the following sections. However, the observations regarding the shape of κ and the ensuing consequences for the complexity of the spectrum are easily explained by the electrostatic analogy. For $s < s_1$ there is an accumulation of charge at the origin (the "spectral condensate", see Fig. 12), this pulls the minimum of the potential to the origin as well, leading to the convex structure of the envelope function (actually, the minimum at the origin appears for $s < s_{1/2}$). As a result, all eigenvalues are real. Once $s > s_{1/2}$ the charges spread out along the axis (see Fig. 12) and the minimum moves away from the origin, leading to a concave envelope function and complex eigenvalues.

===== [10.1] Large s (weak disorder)

When s is large compared with $s_\infty = \sigma$, the density of states of the associated Hermitian matrix is $\rho(x) = N/(\sigma x)$. The integral can be calculated analytically. Specifically, the envelope κ is just the potential along the real axis. The endpoints of the charged bar are

$$a = e^{(s-\sigma)/2}, \quad b = e^{(s+\sigma)/2} \quad (71)$$

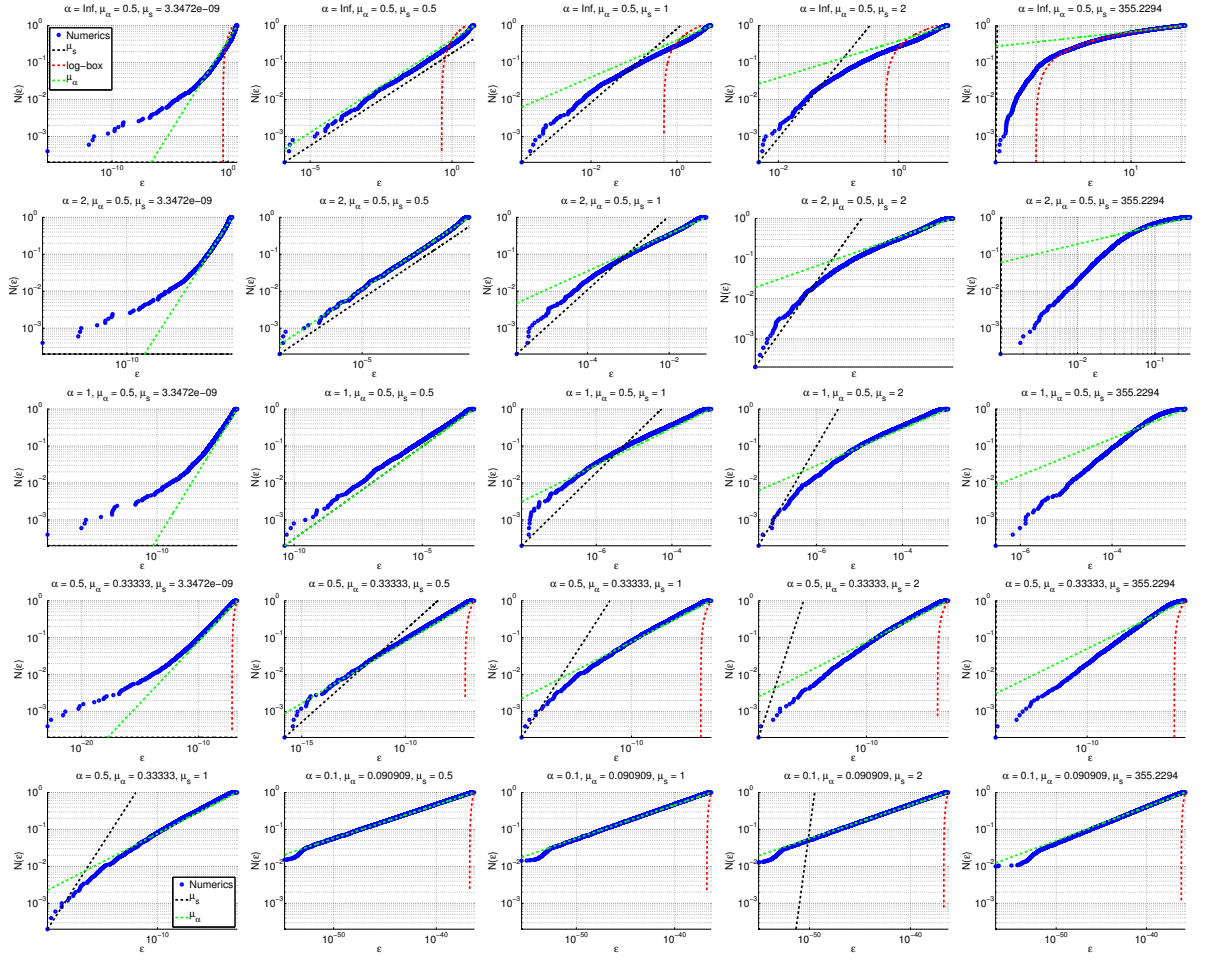


FIG. 14: Integrated density of states. The blue points are calculated from numerical diagonalization. The red line dashed curve corresponds to the log-box result (large s), equation (74). The black dashed-dot line is equation (102) and the green line is just a free particle equation (103). The vertical dotted line is $\epsilon = \exp[(s - \sigma)/2]$.

we obtain

$$[e91] \kappa(x) = \varphi(x, 0) = \frac{1}{\sigma} \int_{e^{(s-\sigma)/2}}^{e^{(s+\sigma)/2}} \frac{\ln(x - x')}{x'} dx' = \quad (72)$$

$$= \ln(|b - x|) \ln\left(\frac{b}{x}\right) + \ln(|x - a|) \ln\left(\frac{x}{a}\right) + \text{Li}_2\left(1 - \frac{b}{x}\right) + \text{Li}_2\left(1 - \frac{a}{x}\right) \quad (73)$$

In Fig. 15 we show the envelope function $\kappa(x)$ along the real axis and the corresponding electrostatic potential and field lines. The potential has a global minimum far from the origin, and a large region of the spectrum is complex. The integrated density of states is

$$[e92] \mathcal{N}(\epsilon) = \frac{N}{\sigma} \left[\ln(\epsilon) - \frac{s - \sigma}{2} \right] \quad (74)$$

Near the origin, the contour $\varphi(x, y) = s/2$ can be approximated by expanding the integrand of equation (65) in x and y and the integrating with respect to x' . The equation $\varphi(x, y) = \varphi(0, 0)$ then is solved by the parabola

$$x = Cy^2 \quad (75)$$

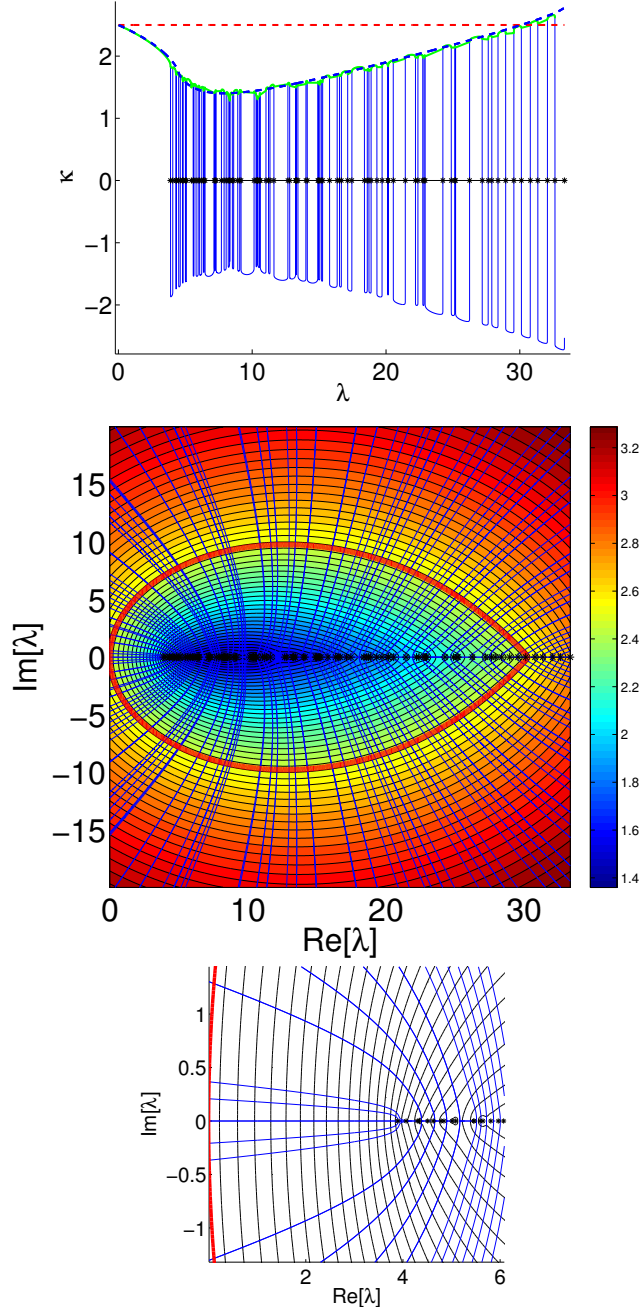


FIG. 15: Top: κ . The green points are the result of numerical diagonalization, the dashed blue line is the analytical result assuming $\rho = (\sigma x)^{-1}$. The stars indicate the position of the "charges", which are the eigenvalues of the associated Hermitian matrix, ε_j . Bottom: Field lines of the corresponding electrostatic problem. The red line is the equipotential line $s/2$. Here $N = 100$ sites, $\sigma = 2$ and $s = 5$.

where the curvature is

$$C \equiv \frac{1}{2} e^{-s/2} \cosh\left(\frac{\sigma}{2}\right) \quad (76)$$

and the gap Δ_λ is given by the expression

$$\int_0^{\sqrt{\Delta_\lambda/C}} |\vec{E}(x, y)| dy = 2\pi \quad (77)$$

This is equivalent, through Cauchy Riemann, to the requirement $\psi(\Delta_\lambda, 0) = 2\pi$. The integrand is approximated by $|\vec{E}(x, y)| \approx |\vec{E}(0, 0)|$ by which we obtain an estimate for the gap

$$[e95] \Delta_\lambda \approx \frac{4\pi^2 C}{\left| \vec{E}(0, 0) \right|^2} = \frac{2\pi^2}{N^2} \exp(s/2 - s_{1/2}) \cosh\left(\frac{\sigma}{2}\right) \quad (78)$$

where the field magnitude at the origin is

$$\left| \vec{E}(0, 0) \right| = |E_x(0, 0)| = \frac{N}{\sigma} \int_a^b \frac{dx}{x^2} = \frac{2N}{\sigma} \sinh\left(\frac{\sigma}{2}\right) e^{-s/2} = Ne^{(s_{1/2}-s)/2} \quad (79)$$

Note that the coulomb integral for the electric field of a wire in two dimensions is

$$E_x = \int_a^b \frac{x - x'}{(x - x')^2 + y^2} \rho(x') dx' \quad (80)$$

$$E_y = \int_a^b \frac{y}{(x - x')^2 + y^2} \rho(x') dx' \quad (81)$$

(82)

and at the origin

$$E_x(0, 0) = \int_a^b \frac{\rho(x)}{x} dx \quad (83)$$

(84)

===== [10.2] The complex gap - Generalization

We expand the potential in a series around the origin

$$\varphi(x, y) = \frac{1}{2} \int_a^b \ln((x - X)^2 + y^2) \rho(X) dX \quad (85)$$

$$\approx \int_a^b \left(\ln(X) - \frac{x}{X} + \frac{1}{2} \frac{y^2}{X^2} + \frac{xy^2}{X^3} \right) \rho(X) dX = \quad (86)$$

$$= C_0 - C_1 x + \frac{1}{2} C_2 y^2 + C_3 x y^2 \quad (87)$$

where the coefficients C_n are defined

$$C_n = \int_a^b \frac{1}{x^n} \rho(x) dx \quad (88)$$

Notice that

$$C_0 = \varphi(0, 0), \quad C_1 = E(0, 0) \quad (89)$$

Since we are interested in the contour $\varphi(x, y) = \varphi(0, 0)$, we obtain

$$x = \frac{C_2}{2C_1} y^2 \quad (90)$$

From equation (78) we obtain the expression

$$[e96] \Delta_\lambda = 2\pi^2 \frac{C_2}{|C_1|^3} \sim \frac{1}{N^2} \frac{(\mu-1)^3}{\mu^2(\mu-2)} \frac{1 - \left(\frac{a}{b}\right)^{\mu-2}}{\left(1 - \left(\frac{a}{b}\right)^{\mu-1}\right)^3} b^{1-2\mu} \quad (91)$$

the last relation is for $\rho(x) \sim N\mu x^{\mu-1}$. I'm not sure about the limit of the integral

===== [10.3] Condition for complexity

For the general density of states

$$\mathcal{N}(x) = \left(\frac{x}{x_c}\right)^\mu \quad (92)$$

The electrostatic potential along the real axis is (integration by parts)

$$V(R) = - \int_0^{x_c} \frac{\mathcal{N}(x)}{x-R} dx \quad (93)$$

The complexity is determined by the slope of the potential at the origin $V(+0)$. The slope is (derivative with respect to R and integrating by parts)

$$V'(R) = \int_0^{x_c} \frac{\mathcal{N}'(x)}{x-R} dx = \frac{\mu}{x_c^\mu} \int_0^{x_c} \frac{x^{\mu-1}}{x-R} dx = \frac{C}{x_c} \quad (94)$$

where $C = x_c V'(R)$. This integral converges for $\mu < 1$. We make the substitution $z = x/R$ under which

$$C = \lim_{z_c \rightarrow \infty} \frac{\mu}{z_c^{\mu-1}} \int_0^{z_c} \frac{z^{\mu-1}}{z-1} dz \quad (95)$$

The integral can be written in terms of Incomplete Euler Beta functions defined as

$$B_u(a, b) = \int_0^u x^{a-1} (1-x)^{b-1} dx \quad (96)$$

However one must be careful and take only the Cauchy principal part

$$I = \int_0^u \frac{x^{\mu-1}}{x-1} dx = \lim_{\varepsilon \rightarrow 0} \left[\int_0^{1-\varepsilon} x^{\mu-1} (1-x)^{-1} + \int_{1+\varepsilon}^u x^{\mu-1} (1-x)^{-1} \right] = \quad (97)$$

$$= \lim_{\varepsilon \rightarrow 0} [B_{1-\varepsilon}(\mu, 0) - B_{1+\varepsilon}(\mu, 0)] = \quad (98)$$

$$= \psi(1-\mu) - \psi(\mu) = \pi \cot(\pi\mu) \quad (99)$$

where $\psi(z)$ is the digamma function and the last equality was obtained by the reflection formula. Two go from the first to second line we made the substitution $t = 1/x$ and took the limit $u \rightarrow \infty$. It is clear that C and thus $V'(+0)$

changes sign from positive to negative at $\mu = 1/2$.

$$V'(R) = \mu \frac{R^\mu}{x_c^\mu} \pi \cot(\pi\mu) \quad (100)$$

===== [10.4] Small s (strong disorder)

For small s , the envelope function increases from zero and is convex. This is due to the fact that there is a "spectral condensate" at $\varepsilon = 0$. We verify this by manually removing the condensate from the spectrum and recalculating the envelope function. In fact, the exact formulas for the integrated density of states $N(E)$ and $\kappa(E)$ in the continuum limit are available due to [8]. We define

$$z = 2304 \frac{D_0^3}{\sigma^4} \varepsilon \quad (101)$$

So the integrated density of states is

$$[e93] \mathcal{N}(z) = \frac{\sigma^2 N}{24\pi^2} \frac{1}{M_\mu^2(\sqrt{z})} \quad (102)$$

Note that in the limit $\varepsilon \rightarrow \infty$ the free particle result is recovered

$$[e94] \mathcal{N}(\varepsilon) = \frac{N}{\pi} \sqrt{\varepsilon} \quad (103)$$

The inverse localization length in [8] is

$$\kappa(z) = -\sqrt{z} \frac{M'_\mu(\sqrt{z})}{M_\mu(\sqrt{z})} \frac{\sigma^2}{48D_0^2}, \quad z \geq 0 \quad (104)$$

where

$$M_\mu(z) = \sqrt{J(z)_\mu^2 + Y(z)_\mu^2} \quad (105)$$

and J_μ and Y_μ are Bessel functions of the first and second kind. In the limit $\varepsilon \rightarrow 0$ we have for $\mu > 0$

$$\mathcal{N}(\varepsilon) \propto N \sigma^{2-4\mu} \varepsilon^\mu \quad (106)$$

$$\rho(\varepsilon) = \frac{d\mathcal{N}}{d\varepsilon} \sim \mu \varepsilon^{\mu-1} \quad (107)$$

$$\kappa(\varepsilon) = \begin{cases} \mu \nearrow 1/2, & \mu < 1/2 \\ \mu \searrow 1/2, & \mu > 1/2 \end{cases} \quad (108)$$

The spectral condensate occurs for $\mu < 1$, however this condition does not ensure that κ has a maximum (global minimum at the origin). The requirement for κ to have a maximum is the more stringent $\mu < 1/2$. At $\mu = 1/2$, κ is flat. Since $\kappa(E \rightarrow \infty) = 1/2$ for all μ , for $\mu > 1/2$ the spectrum becomes entirely complex, whereas in the discrete model only a finite fraction of the eigenvalues can be complex (see Fig. 9).

For $s < s_{1/2}$ the density of state of the hermitian problem and the non hermitian problem are approximately equal (I assume this by observing numerically that Δ_λ vs. Δ_ε for different values of N has a linear correlation). So we can deduce the value of the gap in this region simply by setting $\mathcal{N}(\Delta_\lambda) = 1$ in equation (102)

$$\Delta_\lambda \approx \Delta_\varepsilon = \left(\frac{24\pi^2}{N} \right)^\mu \sigma^{4-2/\mu} \quad (109)$$

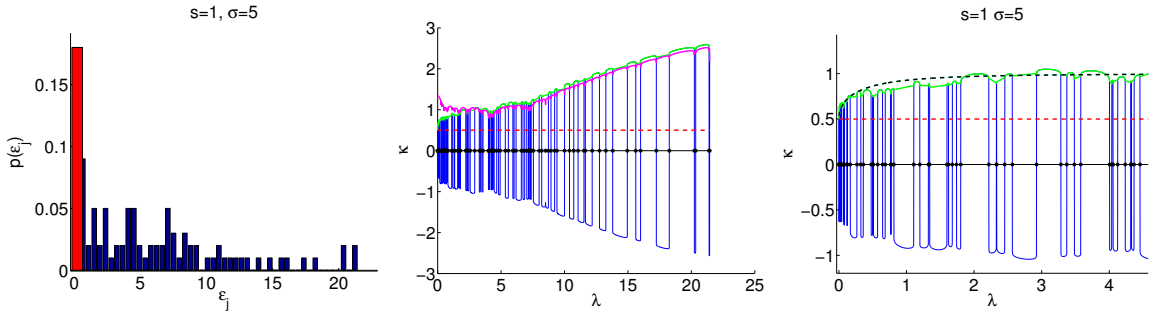


FIG. 16: On the left we show the density of states for $s < s_c$. There is a spectral condensate at the origin (red bar). The envelope function κ is plotted on the right (green line) and it is convex near the origin . If the condensate is removed (magenta) a concave envelope function is obtained. In the bottom figure, we zoom in on the lower band and plot the exact result (dashed black curve).

===== [10.5] The Gap

There are two factors that determine the gap. The distribution of charges and the height of the equipotential contour, namely the value of $s/2$. The distribution of charges determines where the field lines depart from the x -axis and the value $s/2$ determines the "radius" of the contour. For $s_{1/2} < s < s_1$ the departure point and the radius grow together. For $s_1 < s < s_2$, the radius grows but the departure point moves toward the origin. For $s \gg s_2$, they both grow together again.

===== [11] Complexity saturation

The secular equation for the eigenvalues is given by [equation \(70\)](#)

$$\sum_{j=1}^N \log [\lambda - \varepsilon_j(s)] = \log \left[2 \left(\cosh \left(\frac{sN}{2} \right) - 1 \right) \right] \quad (110)$$

where the left hand side is the envelope function $\kappa(\lambda)$. The eigenvalues for which $\kappa(\lambda) > \log [2 (\cosh (\frac{sN}{2}) - 1)]$ are real. In the nonconservative case, one can raise the horizontal line (right hand side of [equation \(70\)](#)) by increasing s , thus making the entire spectrum complex. For a conservative matrix, however, κ is also a function of s , so increasing s raises κ more or less at the same rate, leaving the number of intersections unchanged, see [Fig. 17](#). This claim can be seen from [equation \(70\)](#). Due to the conservative property, the σ disorder is in fact diagonal disorder. Therefore, for large enough s , the eigenvalues of the associated hermitian martix, ε_j grow proportionaly to $\exp(s)$. Increasing $s \rightarrow s + \Delta s$, we have

$$\sum_{j=1}^N \log (\lambda - \varepsilon_j e^{\Delta s}) = \log \left[2 \left(\cosh \left(\frac{(s + \Delta s)N}{2} \right) - 1 \right) \right] \quad (111)$$

$$\sum_{j=1}^N \log (\lambda e^{-\Delta s} - \varepsilon_j) + N\Delta s = \log \left[2 \left(\cosh \left(\frac{sN}{2} \right) - 1 \right) \right] + N\Delta s \quad (112)$$

$$(113)$$

But λ is just a dummy variable, so we can redefine $\lambda := \lambda e^{-\Delta s}$ and the equation is unchanged. Thus increasing s does not change the number of complex solutions.

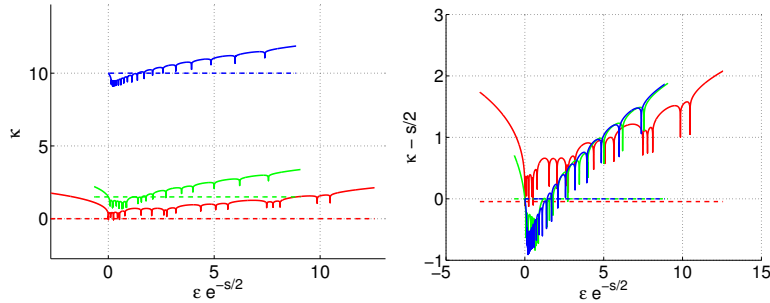


FIG. 17: The inverse localization length κ vs. ε for $N = 20$, $\sigma = 4$, $\Delta = 0$, $s = 0.1$ (red), $s = 3$ (green) and $s = 20$ (blue). The dashed lines are the right hand side of [equation \(70\)](#). In the right panel, the horizontal axis is $\varepsilon e^{-s/2}$ and the vertical axis is $\kappa - s/2$.

===== [11.1] Estimating the fraction of complex eigenvalues

We estimate the the saturation value of the fraction of complex eigenvalues. This means we are interested in the region $s \gg s_\infty$. The eigenvalues have a $\rho \sim 1/x$ distribution and the inverse localization length, $\kappa(x)$ is given by [equation \(72\)](#). Define x_c such that the eigenvalues in the range $\exp[(s - \sigma)/2] < x < x_c$ are complex, x_c is determined by the equation

$$\kappa(x_c) = \frac{s}{2} \quad (114)$$

The fraction of complex eigenvalues is just

$$[e101] n = \frac{\int_a^{x_c} \frac{1}{x} dx}{\int_a^b \frac{1}{x} dx} = \frac{1}{\sigma} \ln \left(\frac{x_c}{a} \right) = \frac{\ln x_c - \frac{s-\sigma}{2}}{\sigma} \quad (115)$$

[11.2] Effect of glassiness on complexity saturation

The effect of glassiness, or offdiagonal disorder (Δ) is to further suppress the complexity, however now the plateau becomes fuzzy, as seen in Fig. 18. This happens because the off diagonal disorder spreads out the eigenvalues as in Fig. 19. For large s , the eigenvalues are approximated by the diagonal elements

$$\varepsilon_j \approx \exp[-B_j + \mathcal{E}_j] \sim \exp\left[-B_j + \frac{s}{2}\right] \quad (116)$$

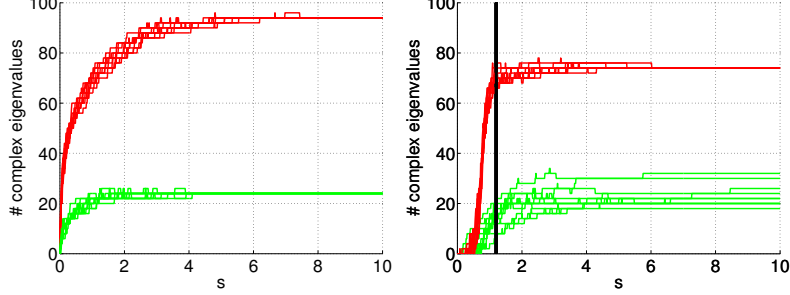


FIG. 18: The number of complex eigenvalues for $\Delta = 1$ (red) and $\Delta = 5$ (green) for $\sigma = 0$ (left panel) and $\sigma = 3$ (right panel).

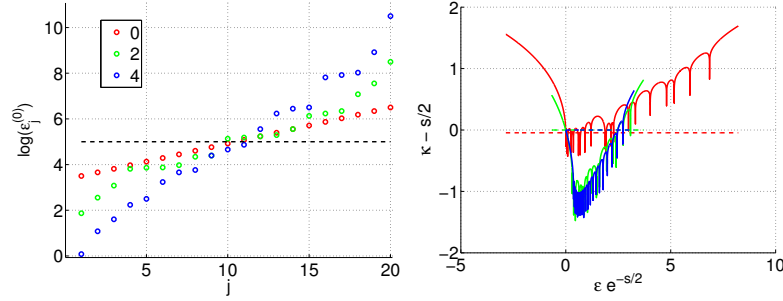


FIG. 19: The eigenvalues $\varepsilon_j^{(0)}$ for $\sigma = 3$ and varying Δ (see legend). As Δ increases, the eigenvalues spread out (left panel), the dashed black horizontal line is $s/2$. As a result, there are more real eigenvalues (right panel).

Excluded material

The following figures show how the spectrum evolves with s , however this is unnecessary due to the electrostatic pictures. However, the figures are illustrative.

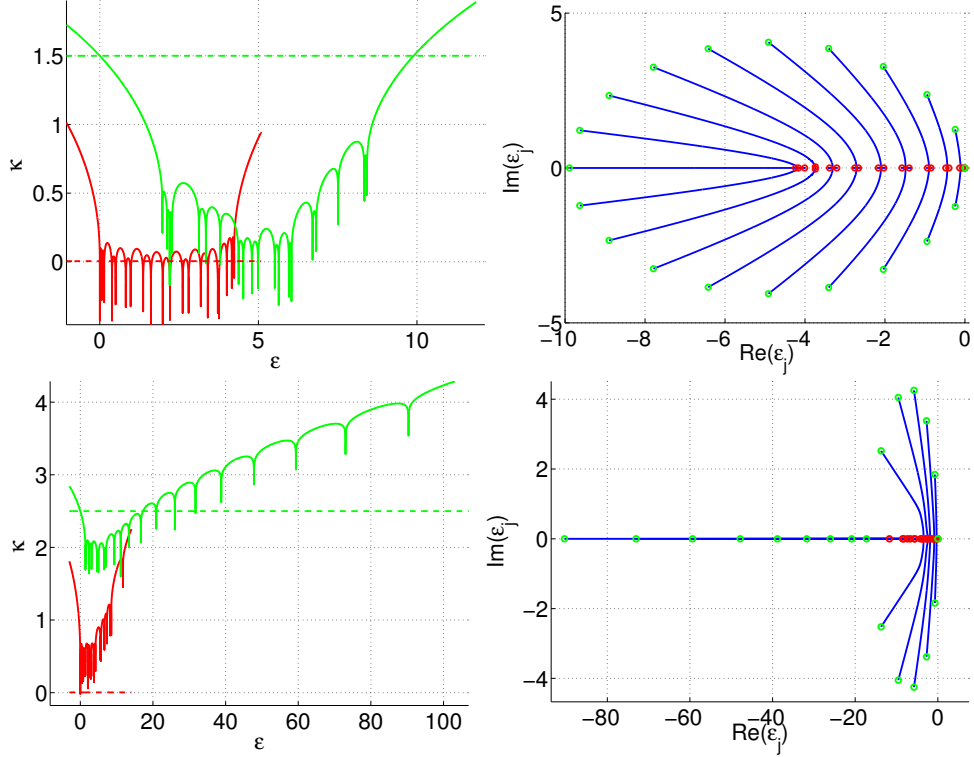


FIG. 20: Top row: The inverse localization length κ vs. ε (left panel) for $N = 20$, $\sigma = 1$, $s = 0.1$ (red) and $s = 3$ (green). The dashed lines are the right hand side of [equation \(70\)](#). For small s all eigenvalues are real, for large s , only two are real. The right panel shows the trajectories of the eigenvalues in the complex plane as s is increased. The green and red dots correspond to the lines of the left panel. Notice that $\varepsilon = 0$ is always a solution. Bottom row: same as top row, but here $\sigma = 4$ and $s = 0.1$ (red) and $s = 5$ (green).

===== [12] Appendix: Secular equation for the clean ring

The wave function can be written

$$\psi(x) = Ae^{ik_+x} + Be^{ik_-x} = e^{\frac{v}{2D}x} \left(Ae^{i\frac{\sqrt{4\lambda D - v^2}}{2D}x} + Be^{-i\frac{\sqrt{4\lambda D - v^2}}{2D}x} \right) \quad (117)$$

Periodic boundary conditions on $\psi(x)$ and $\partial\psi(x)$

$$A + B = Ae^{ik_+L} + Be^{ik_-L} \quad (118)$$

$$ik_+A + ik_-B = ik_+Ae^{ik_+L} + ik_-Be^{ik_-L} \quad (119)$$

Non trivial solutions are given by the equation

$$(k_- - k_+) \left(1 - e^{ik_-L} - e^{ik_+L} - e^{i(k_- + k_+)L} \right) = 0 \quad (120)$$

from which two equations are obtained

$$\cos \left(\sqrt{\frac{4\lambda}{D} - \frac{v^2}{4D^2}} L \right) = \cosh \left(\frac{v}{2D} L \right) \quad (121)$$

===== [13] Appendix: Diffusion equation matching conditions

We consider two types of boundaries. The first case is when there is a jump in the diffusion coefficient. Specifically we are interested in the limit where the jump region a is small and the jump is large. We call this a diffusive scatterer. The second case is a jump in the velocity.

===== [13.1] Diffusive scatterer

The diffusion barrier is defined as

$$D(x) = \begin{cases} D_0, & |x| < a/2 \\ D, & |x| > a/2 \end{cases} \quad (122)$$

Requiring that the diffusion equation [equation \(9\)](#) be continuous dictates that the distribution function $\psi(x)$ and the current $D(x)\partial_x\psi(x) - v\psi(x)$ be continuous. This is in contrast to the Schroedinger equation, where the continuity requirement is on the derivative $\partial_x\psi(x)$ and not on the current. Let us denote the wave function inside the barrier $|x| < a/2$ as ψ_0 . Outside, it is ψ .

$$\psi_0 = Ae^{ik_0x} + Be^{-ik_0x} \quad (123)$$

$$\partial\psi_0 = ik_0(Ae^{ik_0x} - Be^{-ik_0x}) \quad (124)$$

$$(125)$$

where $k_0 = \sqrt{\lambda/D_0}$. Since we will later take the limit $a \rightarrow 0$, we assume that the drift term doesn't play a role within the diffusion barrier.

Inside the barrier, the probability distribution is freely propagating. The values of ψ_0 and $\partial\psi_0$ at each of the boundaries $x = \pm a/2$ can be shown to be related by the linear equation

$$\left(\begin{array}{c} \psi_0 \\ \partial\psi_0 \end{array} \right) \Big|_{-a/2} = \left(\begin{array}{cc} \cos(k_0a) & \frac{1}{k_0} \sin k_0a \\ -k_0 \sin k_0a & \cos(k_0a) \end{array} \right) \left(\begin{array}{c} \psi_0 \\ \partial\psi_0 \end{array} \right) \Big|_{a/2} \quad (126)$$

And requiring continuity of the distribution and the current, we can stitch the interior solution ψ_0 to the exterior solution ψ

$$\left(\begin{array}{c} \psi \\ \partial\psi \end{array} \right) \Big|_{-a/2} = \left(\begin{array}{cc} \cos(k_0 a) & \frac{D}{D_0 k_0} \sin k_0 a \\ -\frac{D_0 k_0}{D} \sin k_0 a & \cos(k_0 a) \end{array} \right) \left(\begin{array}{c} \psi \\ \partial\psi \end{array} \right) \Big|_{a/2} \quad (127)$$

Taking, carefully, the limit $a \rightarrow 0$,

$$\left(\begin{array}{c} \psi \\ \partial\psi \end{array} \right) \Big|_{-a/2} \approx \left(\begin{array}{cc} 1 & D \frac{a}{D_0} \\ 0 & 1 \end{array} \right) \left(\begin{array}{c} \psi \\ \partial\psi \end{array} \right) \Big|_{a/2} \quad (128)$$

rewriting these two equations explicitly, we obtain the diffusion barrier matching conditions

$$[e61] \psi(a/2) - \psi(-a/2) = -\frac{a}{D_0} D \partial\psi(a/2) \quad (129)$$

$$\partial\psi(a/2) = \partial\psi(-a/2) \quad (130)$$

To check, notice that if $D_0 \rightarrow 0$ faster than $a \rightarrow 0$, Neumann boundary conditions are recovered.

If $D_0 = D$, periodic boundary conditions are recovered. The matching conditions of equation (129) can be written in matrix form with the matching matrix M

$$M = \left(\begin{array}{cc} 1 & D \frac{a}{D_0} \\ 0 & 1 \end{array} \right) \quad (131)$$

Let us define

$$\alpha = \frac{a}{D_0}, \quad g = \frac{a}{L} \cdot \frac{D}{D_0} \quad (132)$$

as the strength of the diffusion barrier, in analogy with a delta function potential $u\delta(x)$ in the Schroedinger equation.

===== [13.2] Jump in the velocity

The velocity $v(x)$ in the diffusion equation is

$$v(x) = \begin{cases} v_1, & 0 < x < L/2 \\ v_2, & L/2 < x < L \end{cases} \quad (133)$$

with

$$v_1 = s_1 D = D(s + \sigma) \quad (134)$$

$$v_2 = s_2 D = D(s - \sigma) \quad (135)$$

Continuity of the diffusion equation across the boundaries requires that the distribution ψ and the current $D\partial\psi - v\psi$ be continuous across the boundaries

$$\left(\begin{array}{c} \psi_1 \\ \partial\psi_1 \end{array} \right) = M(v_1 - v_2) \left(\begin{array}{c} \psi_2 \\ \partial\psi_2 \end{array} \right) \quad (136)$$

where

$$M(u) \equiv \left(\begin{array}{cc} 1 & 0 \\ \frac{u}{D} & 1 \end{array} \right) \quad (137)$$

[14] Appendix: Secular equation for ring + g

The transfer matrix across a segment of length $L/2$ is

$$T(s, k; L/2) \equiv \frac{e^{sL/4}}{k} \begin{pmatrix} -\frac{s}{2} \sin\left(\frac{kL}{2}\right) + k \cos\left(\frac{kL}{2}\right) & \sin\left(\frac{kL}{2}\right) \\ -\left(\frac{s^2}{4} + k^2\right) \sin\left(\frac{kL}{2}\right) & \frac{s}{2} \sin\left(\frac{kL}{2}\right) + k \cos\left(\frac{kL}{2}\right) \end{pmatrix} \quad (138)$$

Using the matching conditions of [equation \(129\)](#) and the solution of the form of [equation \(13\)](#), together with periodic boundary conditions, we have

$$\left. \begin{pmatrix} \psi \\ \partial\psi \end{pmatrix} \right|_{x=0} = TMT \left. \begin{pmatrix} \psi \\ \partial\psi \end{pmatrix} \right|_{x=0} \quad (139)$$

A non trivial solution is possible only if

$$\det(TMT - I) = 0 \quad (140)$$

which leads to the secular equation

$$[\text{e71}] \cos(\tilde{k}L) + \alpha \frac{\lambda}{2\tilde{k}} \sin(\tilde{k}L) = \cosh(sL/2) \quad (141)$$

which can also be written simply as

$$\sqrt{1 + \alpha^2 \frac{\lambda^2}{4\tilde{k}^2}} \cos \left[\tilde{k}L - \arctan \left(\alpha \frac{\lambda}{2\tilde{k}} \right) \right] = \cosh(sL/2) \quad (142)$$

where

$$\tilde{k} \equiv k + \frac{is}{2} = \sqrt{\frac{\lambda}{D} - \frac{s^2}{4}} \quad (143)$$

In more conventional notations, [equation \(141\)](#) can be written as follows

$$[\text{e81}] \cos(\gamma(\lambda)) = \sqrt{g(\lambda)} \cosh \left(\frac{sL}{2} \right) \quad (144)$$

where

$$g(\lambda) = \left[1 + \left(\frac{\lambda}{2\tilde{k}} \alpha \right)^2 \right]^{-1}, \quad \gamma(\lambda) = \tilde{k}L - \arctan \left(\frac{\lambda}{2\tilde{k}} \alpha \right) \quad (145)$$

[15] Appendix: Secular equation for ring+ σ

Details of the derivation of [equation \(36\)](#) and [equation \(38\)](#) are as follows: The diffusion equation with space dependent drift is

$$[\text{e15}] \frac{\partial\psi}{\partial t} = D \frac{\partial^2\psi}{\partial x^2} - \frac{\partial}{\partial x} [v(x)\psi] \quad (146)$$

with

$$v(x) = \begin{cases} v_1, & 0 < x < L/2 \\ v_2, & L/2 < x < L \end{cases} \quad (147)$$

and

$$v_1 = s_1 D = D(s + \sigma) \quad (148)$$

$$v_2 = s_2 D = D(s - \sigma) \quad (149)$$

The solutions are of the form $\psi \sim e^{-\lambda t + ikx}$. In each region (1, 2) we have two k 's, \pm :

$$k_{1,2}^{\pm} = \frac{-iv_{1,2} \pm \sqrt{4\lambda D - v_{1,2}^2}}{2D} = -\frac{is_{1,2}}{2} \pm \sqrt{\frac{\lambda}{D} - \frac{s_{1,2}^2}{4}} \equiv -\frac{is_{1,2}}{2} \pm k_{1,2} \quad (150)$$

In each region we may write the solution, i.e.:

$$\psi_1(x) = Ae^{ik_1^+ x} + Be^{ik_1^- x} \quad (151)$$

$$\partial_x \psi_1(x) = ik_1^+ A e^{ik_1^+ x} + ik_1^- B e^{ik_1^- x} \quad (152)$$

From which we can obtain the connection between $(\psi, \partial\psi)$ at any two points, specifically for the boundaries of the region $[0, L/2]$ we have

$$\left(\begin{array}{c} \psi_1 \\ \partial\psi_1 \end{array} \right) \Big|_{x=0} = T(s_1, k_1) \left(\begin{array}{c} \psi_1 \\ \partial\psi_1 \end{array} \right) \Big|_{x=L/2} \quad (153)$$

where

$$T(s, k; L/2) \equiv \frac{e^{sL/4}}{k} \begin{pmatrix} -\frac{s}{2} \sin\left(\frac{kL}{2}\right) + k \cos\left(\frac{kL}{2}\right) & \sin\left(\frac{kL}{2}\right) \\ -\left(\frac{s^2}{4} + k^2\right) \sin\left(\frac{kL}{2}\right) & \frac{s}{2} \sin\left(\frac{kL}{2}\right) + k \cos\left(\frac{kL}{2}\right) \end{pmatrix} \quad (154)$$

Continuity of the diffusion equation across the boundaries requires that the distribution ψ and the current $D\partial\psi - v\psi$ be continuous across the boundaries

$$\left(\begin{array}{c} \psi_1 \\ \partial\psi_1 \end{array} \right) \Big|_{x=L/2} = M(v_1 - v_2) \left(\begin{array}{c} \psi_2 \\ \partial\psi_2 \end{array} \right) \Big|_{x=L/2} \quad (155)$$

where

$$M(u) \equiv \begin{pmatrix} 1 & 0 \\ \frac{u}{D} & 1 \end{pmatrix} \quad (156)$$

To find λ , we apply these transformations along the entire segment $[0, L]$ and impose periodic boundary conditions

$$\left(\begin{array}{c} \psi_1 \\ \partial\psi_1 \end{array} \right) \Big|_{x=0} = T(s_1, k_1) M(v_1 - v_2) T(s_2, k_2) M(v_2 - v_1) \left(\begin{array}{c} \psi_1 \\ \partial\psi_1 \end{array} \right) \Big|_{x=0} \quad (157)$$

This equation has a non trivial solution only if

$$\det [I - T(s_1, k_1) M(v_1 - v_2) T(s_2, k_2) M(v_2 - v_1)] = 0 \quad (158)$$

leading to the secular equation

$$\cosh\left(\frac{sL}{2}\right) = \cos\left(\frac{L}{4}\sqrt{4\lambda - (s-\sigma)^2}\right)\cos\left(\frac{L}{4}\sqrt{4\lambda - (s+\sigma)^2}\right) - \quad (159)$$

$$- \frac{(4\lambda - s^2 + \sigma^2)}{\sqrt{4\lambda - (s-\sigma)^2}\sqrt{4\lambda - (s+\sigma)^2}} \sin\left(\frac{L}{4}\sqrt{4\lambda - (s-\sigma)^2}\right) \sin\left(\frac{L}{4}\sqrt{4\lambda - (s+\sigma)^2}\right) \quad (160)$$

We Define k as in the $\sigma = 0$ case, such that

$$\lambda = D\left(k^2 + \frac{s^2}{4}\right) = \frac{D}{L^2}\left(z^2 + \frac{\mathcal{S}^2}{4}\right) \quad (161)$$

$$z \equiv kL, \quad \mathcal{S} \equiv sL, \quad \sigma := \sigma L \quad (162)$$

where $z = x + iy$ is complex and write the secular equation as

$$\begin{aligned} \cosh\left(\frac{\mathcal{S}}{2}\right) &= \cos\left[\frac{1}{2}\sqrt{z^2 - \left(\frac{\sigma}{2}\right)^2 - \frac{\sigma\mathcal{S}}{2}}\right]\cos\left[\frac{1}{2}\sqrt{z^2 - \left(\frac{\sigma}{2}\right)^2 + \frac{\sigma\mathcal{S}}{2}}\right] - \\ &- \left(z^2 + \left(\frac{\sigma}{2}\right)^2\right) \frac{\sin\left[\frac{1}{2}\sqrt{z^2 - \left(\frac{\sigma}{2}\right)^2 - \frac{\sigma\mathcal{S}}{2}}\right]}{\sqrt{z^2 - \left(\frac{\sigma}{2}\right)^2 - \frac{\sigma\mathcal{S}}{2}}} \frac{\sin\left[\frac{1}{2}\sqrt{z^2 - \left(\frac{\sigma}{2}\right)^2 + \frac{\sigma\mathcal{S}}{2}}\right]}{\sqrt{z^2 - \left(\frac{\sigma}{2}\right)^2 + \frac{\sigma\mathcal{S}}{2}}} \end{aligned} \quad (163)$$

[16] Appendix: Eigenvalue equation for disordered ring

The method described here appears in various forms in [11, 21], it is known as the "Hatano - Nelson" method.

We define $\Gamma^{(s)} \equiv -\tilde{W}$, where \tilde{W} is the rate matrix after gauging away the disorder,

$$\Gamma^{(s)} = \text{diag}[\gamma] + \text{offdiag}[-ge^{\pm s/2}] = \quad (164)$$

$$= \begin{pmatrix} \gamma_1 & -g_1 e^{s/2} & & -g_N e^{-s/2} \\ -g_1 e^{-s/2} & \ddots & \ddots & \\ & \ddots & \ddots & -g_{N-1} e^{s/2} \\ -g_n e^{s/2} & & -g_{N-1} e^{-s/2} & \gamma_N \end{pmatrix} \quad (165)$$

where the decay rates (include the disorder!!)

$$\gamma_n = g_{n-1} e^{-(s+\sigma_{n-1})/2} + g_n e^{(s+\sigma_n)/2} \quad (166)$$

The eigenvalues of Γ are solutions to the equation

$$\det(\Gamma^{(s)} - \lambda I) = 0 \quad (167)$$

The associated hermitian matrix is

$$H = \text{diag}[\gamma] + \text{offdiag}[-g] \quad (168)$$

and it has real eigenvalues ε_j . This determinant can be calculated using a formula due to Molinari [21] for tridiagonal matrices. We define the matrix [check the indices... go over the convention with Doron]

$$T^{(n)} = \begin{pmatrix} \gamma_n - \lambda & -g_{n-1}^2 \\ 1 & 0 \end{pmatrix} \quad (169)$$

The key point is that the matrices T_n are the same for $\Gamma^{(s)}$ and for H . Using the formula for the determinant for both matrices, we obtain

$$\det(H - \lambda I) = \text{tr} \left[\prod_{n=1}^N T_n \right] - 2 \left[\prod_{n=1}^N g_n \right] \quad (170)$$

$$\det(\Gamma^{(s)} - \lambda I) = \text{tr} \left[\prod_{n=1}^N T_n \right] - 2 \left[\prod_{n=1}^N g_n \right] \cosh \left(\frac{sN}{2} \right) \quad (171)$$

$$(172)$$

subtracting the equations and writing the characteristic polynomial of the Hermitian matrix

$$\det(H - \lambda I) = \prod_{n=1}^N (\varepsilon_n - \lambda) \quad (173)$$

we obtain an equation for the eigenvalues λ

$$\prod_{n=1}^N (\lambda - \varepsilon_n) = \left[\prod_{n=1}^N g_n \right] 2 \left(\cosh \left(\frac{sN}{2} \right) - 1 \right) \quad (174)$$

According to Thouless, for the corresponding Hermitian problem

$$e^{N/\xi} = \prod_{n=1}^N \frac{\lambda - \varepsilon_n}{g_n} \quad (175)$$

where $\kappa = 1/\xi$ is the inverse localization length.

===== [17] Appendix: Anderson localization and Thouless

The FGR approximation for the inverse localization length in the case of diagonal disorder is

$$\kappa(E) = \frac{\sigma^2}{24(4 - E^2)} \quad (176)$$

where $E := E - \langle e^x \rangle$ and $x \in [-\sigma/2, \sigma/2]$.

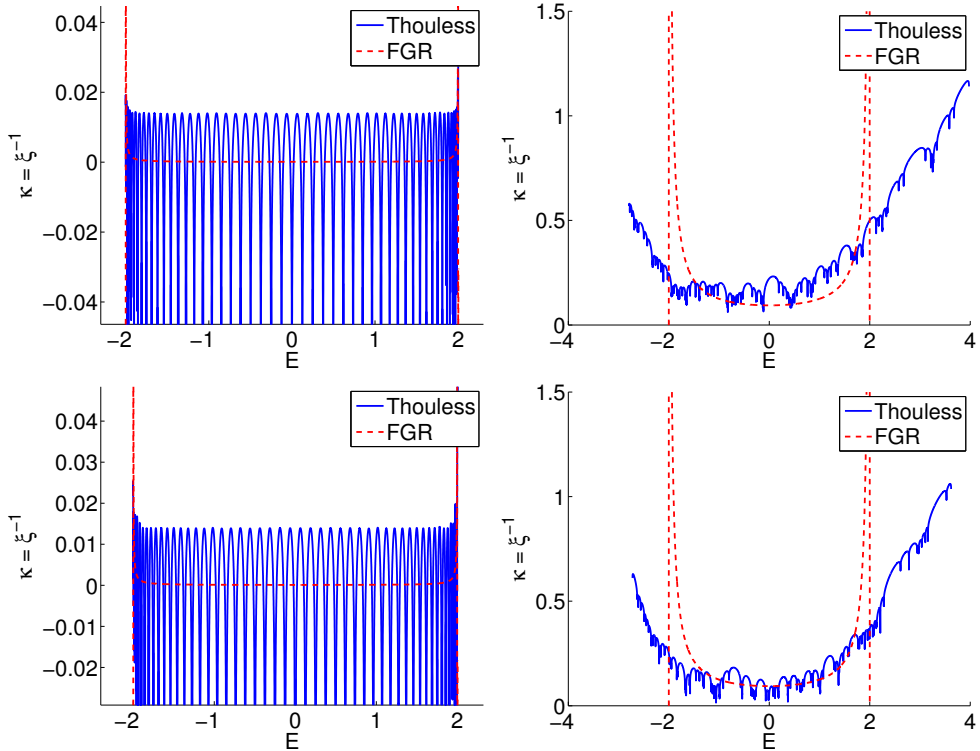


FIG. 21: First row: Anderson model with uncorrelated box distribution noise, $\sigma = 0.1$ (left) and $\sigma = 3$ (right)
Second row: Anderson model with uncorrelated log-box distribution noise, $\sigma = 0.1$ (left) and $\sigma = 3$ (right). Notice that the mean was subtracted from the diagonal! N=100.

[18] Interplay between resistor network and Sinai: Drift and diffusion

We calculate the drift velocity v and the diffusion coefficient D as a function of the affinity s . In the absence of disorder ($\Delta = \sigma = 0$) they are related by a *generalized* Einstein relations:

$$\frac{v}{D} = \frac{2}{a} \tanh\left(\frac{as}{2}\right) \quad (177)$$

where $a = 1$ is the lattice constant. The traditional Einstein relation $v/D = s$ holds if s is sufficiently small. This is usually rephrased as mobility/diffusion = $1/T$. The other extreme limit of very large s implies unidirectional transitions with $v/D = 2/a$. The latter ratio reflects Poisson statistics.

Taking the disorder into account the Poisson limit becomes $v/D = 2/a_\infty$, where a_∞ depends on the disorder:

$$[e4] a_\infty = \left(\frac{2D}{v} \right)_{s \rightarrow \infty} = \left[\frac{\langle (1/\vec{w})^2 \rangle}{\langle (1/\vec{w}) \rangle^2} \right] = \frac{\sigma \Delta}{4} \coth\left(\frac{\sigma}{2}\right) \coth\left(\frac{\Delta}{2}\right) \quad (178)$$

If we increase s from zero to infinity the ratio v/D has a crossover from $v/D = s$ to $v/D = 2/a_\infty$, which is illustrated in Fig. 22. Due to the disorder σ we get what we call a “Sinai step”. This means that for small s the transport is suppressed due to the buildup of a potential barrier, while large enough s flattens the barrier leading to “sliding” with large drift velocity.

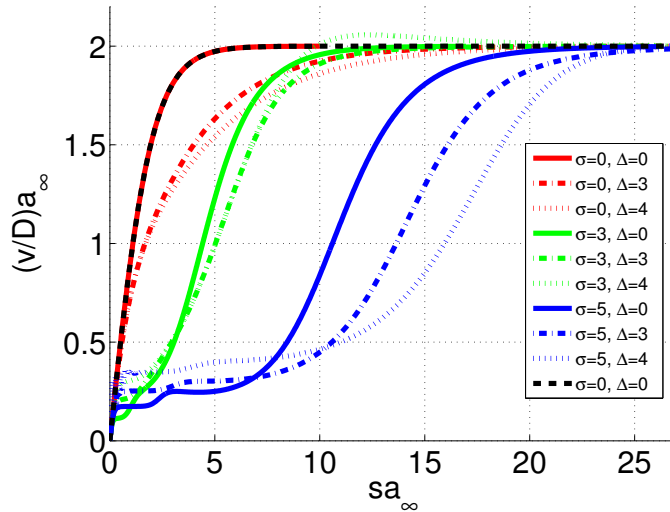


FIG. 22: The scaled v/D ratio versus the scaled s for various values of σ and Δ . Different colors correspond to different σ , while different line styles correspond to different Δ . The dashed black line $2 \tanh(x)$ describes the result that would be obtained for a non-disordered model. The number of sites is $N = 30$.

The additional aspect that we want to analyze is the implication of having log-wide distribution of couplings, i.e. having finite Δ . We observe in Fig. 22 that by increasing Δ the Sinai step is somewhat smeared: the crossover from activated transport to sliding becomes wider.

In order to get the “big picture” we calculate the ratio between the scaled v/D and the reference curve $2 \tanh(x)$ and displays the results as images in Fig. 23. The small s results imply that Δ has little effect on the beginning of the Sinai step. Namely it hardly affects the crossover from the linear-response (Einstein) regime to the activated transport (Sinai) regime. But the effect of Δ becomes qualitatively similar to the effect of σ as we cross from activated transport to “sliding”.

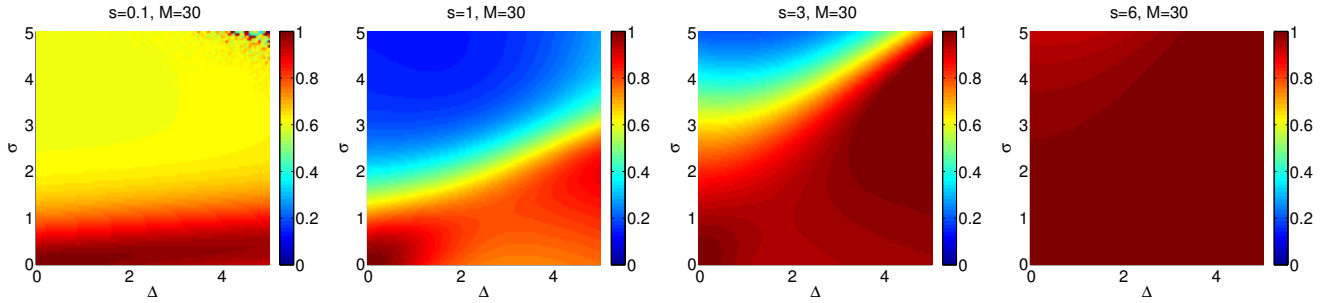


FIG. 23: The ratio between $a_\infty v/D$ and $2 \tanh(x)$ is imaged as a function of Δ and σ for representative values of the affinity ($s = 0.1, 1, 3, 6$). The number of sites is $N = 30$.

===== [19] A more detailed analysis

To determine the roles played by σ and Δ , we study the probability distribution of the displacement x . In the ring context it is defined as the winding number times N . We look at the cumulant generating function

$$[e3] g(\lambda) = \lim_{t \rightarrow \infty} \left[-\frac{1}{t} \ln \langle e^{-\lambda x} \rangle_t \right] \quad (179)$$

which completely determines the probability distribution in the long time limit. Note that $g(\lambda)$ satisfies the non equilibrium fluctuation theorem (NFT)

$$g(\lambda) = g(s - \lambda) \quad (180)$$

If the distribution is Gaussian, then $g(\lambda)$ is a parabola

$$g(\lambda) = v\lambda - D\lambda^2 \quad (181)$$

and the NFT implies $v/D = s$. This parabola has a maximum at $\lambda = (1/2)v/D$ with height

$$h = \max[g(\lambda)] = \frac{v^2}{4D} = \frac{1}{4}vs \quad (182)$$

Accordingly we use the following dimensionless parameters in order to characterize the deviation from Gaussian statistics:

$$\frac{v/D}{s} \text{ and } 4 \frac{h/v}{s} \quad [\text{both equal unity for Gaussian statistics}] \quad (183)$$

In Fig. 24 these two parameters are imaged as a function of Δ and σ for representative values of s . For small values of s , the ratio v/Ds is quite independent of Δ , while as s increases, the effect of Δ becomes more significant.

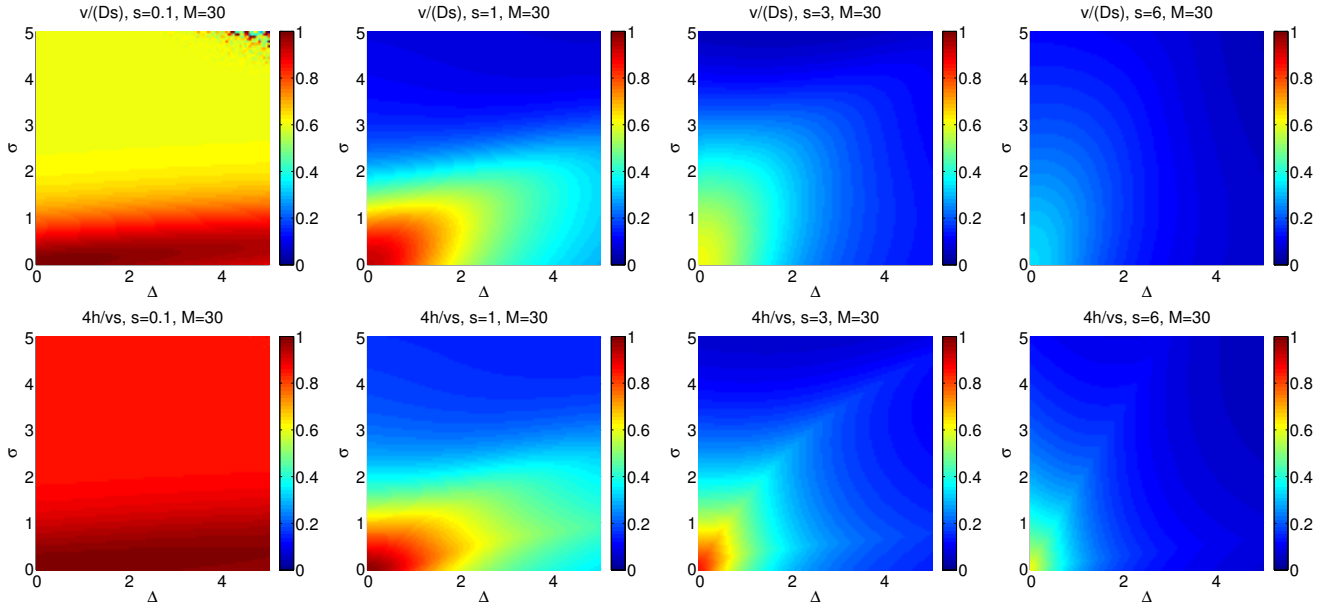


FIG. 24: The measures for Gaussian statistics are imaged as a function of Δ and σ for representative values of s .

===== [20] The shape of $g(\lambda)$

Given v and D , the parabola is defined and it has a peak value of

$$h[\text{Gaussian}] = v^2/4D \quad (184)$$

In general, however, the peak value is different. In the Poisson limit, $s \rightarrow \infty$, it is easy to show that the minimum of the generating function is given by the smallest transition rate

$$h[\text{Poisson}] = \min[\vec{w}_n] \quad (185)$$

If there is no disorder, the cumulant generating function can easily be shown to be

$$g(\lambda) = \vec{w} e^{\lambda a} + \overleftarrow{w} e^{-\lambda a} - (\overleftarrow{w} + \vec{w}) \quad (186)$$

For zero bias ($s = 0$) this reduces to

$$g(\lambda) = 2w(\cosh(\lambda a) - 1) \quad (187)$$

We emphasize that even in the absence of disorder and zero bias, the distribution is not Gaussian, due to having a discrete lattice (Fig. 25).

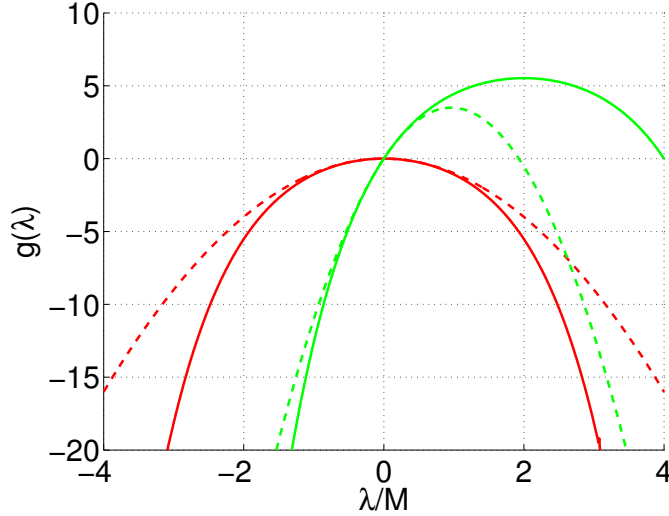


FIG. 25: The effect of discretization on the generating function $g(\lambda)$. The red line is for $s = 0$, the green line is for $s = 4$. In both cases $\sigma = 0$ and $\Delta = 0$. Dashed lines are parabolas $v\lambda - D\lambda^2$.

===== [21] Appendix: Summary of main results in [8]

Master equation on a lattice with spacing a and transition rates

$$W_{n,n+1} = \frac{D_0}{a^2} \exp \left[-a \frac{F_{n+1}}{2kT} \right] \quad (188)$$

$$W_{n+1,n} = \frac{D_0}{a^2} \exp \left[a \frac{F_{n+1}}{2kT} \right] \quad (189)$$

The random force on the bond $(n-1, n)$ is F_n and distributed according to a gaussian such that

$$\langle F_n \rangle = F_0, \quad \langle F_n F_m \rangle - F_0^2 = \frac{\sigma}{a} \delta_{n,m} \quad (190)$$

Scaled affinity

$$\mu = \frac{2F_0 T}{\sigma} \quad (191)$$

Length and time scales are expressed in natural units of

$$x_1 = \frac{4D_0^2}{\sigma}, \quad \tau_1 = \frac{8D_0^3}{\sigma^2} \quad (192)$$

References:

- [1] A. Amir, Y. Oreg, and Y. Imry, “On relaxations and aging of various glasses,” *Proceedings of the National Academy of Sciences*, vol. 109, no. 6, pp. 1850–1855, 2012.
- [2] A. Vaknin, Z. Ovadyahu, and M. Pollak, “Aging effects in an anderson insulator,” *Phys. Rev. Lett.*, vol. 84, pp. 3402–3405, Apr 2000.
- [3] A. Amir, Y. Oreg, and Y. Imry, “Slow relaxations and aging in the electron glass,” *Phys. Rev. Lett.*, vol. 103, p. 126403, Sep 2009.
- [4] Y. de Leeuw and D. Cohen, “Diffusion in sparse networks: Linear to semilinear crossover,” *Phys. Rev. E*, vol. 86, p. 051120, Nov 2012.
- [5] J.-P. Bouchaud and A. Georges, “Anomalous diffusion in disordered media: Statistical mechanisms, models and physical applications,” *Physics Reports*, vol. 195, no. 45, pp. 127 – 293, 1990.
- [6] Y. G. Sinai, “Limit behaviour of one-dimensional random walks in random environments,” *Teoriya Veroyatnostei i ee Primeneniya*, vol. 27, no. 2, pp. 247–258, 1982.
- [7] B. Derrida, “Velocity and diffusion constant of a periodic one-dimensional hopping model,” *Journal of Statistical Physics*, vol. 31, no. 3, pp. 433–450, 1983.
- [8] J. Bouchaud, A. Comtet, A. Georges, and P. L. Doussal, “Classical diffusion of a particle in a one-dimensional random force field,” *Annals of Physics*, vol. 201, no. 2, pp. 285 – 341, 1990.
- [9] N. Hatano and D. R. Nelson, “Localization transitions in non-hermitian quantum mechanics,” *Phys. Rev. Lett.*, vol. 77, pp. 570–573, Jul 1996.
- [10] N. Hatano and D. R. Nelson, “Vortex pinning and non-hermitian quantum mechanics,” *Phys. Rev. B*, vol. 56, pp. 8651–8673, Oct 1997.
- [11] N. M. Shnerb and D. R. Nelson, “Winding numbers, complex currents, and non-hermitian localization,” *Phys. Rev. Lett.*, vol. 80, pp. 5172–5175, Jun 1998.
- [12] P. W. Brouwer, P. G. Silvestrov, and C. W. J. Beenakker, “Theory of directed localization in one dimension,” *Phys. Rev. B*, vol. 56, pp. R4333–R4335, Aug 1997.
- [13] I. Y. Goldsheid and B. A. Khoruzhenko, “Distribution of eigenvalues in non-hermitian anderson models,” *Phys. Rev. Lett.*, vol. 80, pp. 2897–2900, Mar 1998.
- [14] J. Feinberg and A. Zee, “Non-hermitian localization and delocalization,” *Phys. Rev. E*, vol. 59, pp. 6433–6443, Jun 1999.
- [15] D. K. Lubensky and D. R. Nelson, “Pulling pinned polymers and unzipping dna,” *Phys. Rev. Lett.*, vol. 85, pp. 1572–1575, Aug 2000.
- [16] D. K. Lubensky and D. R. Nelson, “Single molecule statistics and the polynucleotide unzipping transition,” *Phys. Rev. E*, vol. 65, p. 031917, Mar 2002.
- [17] D. R. Nelson and N. M. Shnerb, “Non-hermitian localization and population biology,” *Phys. Rev. E*, vol. 58, pp. 1383–1403, Aug 1998.
- [18] Y. Kafri, D. K. Lubensky, and D. R. Nelson, “Dynamics of molecular motors and polymer translocation with sequence heterogeneity,” *Biophysical Journal*, vol. 86, no. 6, pp. 3373 – 3391, 2004.
- [19] Y. Kafri, D. K. Lubensky, and D. R. Nelson, “Dynamics of molecular motors with finite processivity on heterogeneous tracks,” *Phys. Rev. E*, vol. 71, p. 041906, Apr 2005.
- [20] J. T. Chalker and Z. J. Wang, “Diffusion in a random velocity field: Spectral properties of a non-hermitian fokker-planck operator,” *Phys. Rev. Lett.*, vol. 79, pp. 1797–1800, Sep 1997.
- [21] L. G. Molinari, “Determinants of block tridiagonal matrices,” *Linear Algebra and its Applications*, vol. 429, no. 89, pp. 2221 – 2226, 2008.